To link to this article : DOI:10.1016/j.jcp.2014.02.037
http://dx.doi.org/10. 1016/j.jcp.2014.02.037

Numerical computation of 3D heat transfer in complex parallel heat exchangers using generalized Graetz modes

Charles Pierre [a], Julien Bouyssier [b], Frédéric de Gournay [d], Franck Plouraboué [b,c,*]

[a] Laboratoire de Mathématiques et Applications de Pau, CNRS and Université de Pau et du Pays de l'Adour, av. de l'Université, 64013 Pau Cedex, France
[b] Université de Toulouse, INPT, UPS, IMFT (Institut de Mécanique des Fluides de Toulouse), Allés Camille Soula, F-31400 Toulouse, France
[c] CNRS, IMFT, F-31400 Toulouse, France
[d] Institut de Mathématiques de Toulouse, CNRS and Université Paul Sabatier, Toulouse, France

A B S T R A C T

We propose and develop a variational formulation dedicated to the simulation of parallel convective heat exchangers that handles possibly complex input/output conditions as well as connection between pipes. It is based on a spectral method that allows to re-cast three-dimensional heat exchangers into a two-dimensional eigenvalue problem, named the generalized Graetz problem. Our formulation handles either convective, adiabatic, or prescribed temperature at the entrance or at the exit of the exchanger. This formulation is robust to mode truncation, offering a huge reduction in computational cost, and providing insights into the most contributing structure to exchanges and transfer. Several examples of heat exchangers are analyzed, their numerical convergence is tested and the numerical efficiency of the approach is illustrated in the case of Poiseuille flow in tubes.

Keywords:
Generalized Graetz mode
Parallel heat exchangers
Optimal weak-variational formulation
Functional minimization

1. Introduction

1.1. Motivation, context, and brief overview

Parallel convective heat exchangers are relevant in various applications such as heating or cooling systems [1], and convective heat exchangers [2]. Since the seminal contributions of Nunge et al. [3,4] there has been a number of works devoted to parallel convective heat exchangers in simple two-dimensional (2D) configurations among which [5–10] to cite only a few, whilst many other can be found in a recent review [11]. As quoted in [11] conjugate heat transfer are mixed parabolic/hyperbolic problems which makes them numerically challenging.

Many previous analysis of conjugate heat transfer have limited their interest to two-dimensional configurations (either planar or axi-symmetrical) and convection dominated situations for which the longitudinal conduction is neglected in the fluid but also in the solid region. The first restriction is mostly associated with the computational cost when dealing with realistic three-dimensional (3D) configurations. The increase in computer power permits the use of standard finite volume

* Corresponding author at: Université de Toulouse, INPT, UPS, IMFT (Institut de Mécanique des Fluides de Toulouse), Allés Camille Soula, F-31400 Toulouse, France.
E-mail addresses: charles.pierre@univ-pau.fr (C. Pierre), jbouyssi@imft.fr (J. Bouyssier), frederic@degournay.fr (F. de Gournay), fplourab@imft.fr (F. Plouraboué).

or finite difference methods to obtain 3D solutions in order to predict heat exchangers performances [12–16]. Nevertheless, numerical precision can become an issue in certain parameter range and more elaborated numerical methods have been proposed to solve conjugate heat transfer computations, e.g. using SIMPLE -algorithm with finite volume in 2D [17] or dual reciprocity boundary element methods [18–20] to tackle 3D problems.

Furthermore, the focus on convection-dominated situations, albeit justified for traditional convective heat exchangers, has to be reconsidered when dealing with applications such as micro-heat exchangers, where longitudinal conduction plays a non-negligible role. This last point, as secondary as it might appear, takes on fundamental implications from the theoretical point of view. First, it has been a recurrent hindrance for the generalization of Graetz modes as discussed in detail in [21]. Secondly, it brings new questions concerning the modeling of convective heat exchangers, since convective outlet boundary conditions are generally used in this context to describe an approximated purely hyperbolic problem in the longitudinal direction.

Convective boundary conditions, i.e. in finite difference solutions, propagating the penultimate temperature value of the considered discrete mesh at the boundary as in [12–14], permits to circumvent the intrinsic free-boundary nature of heat exchangers outlet. However the temperature value at the outlet not only depends on the inlet value, but also on the total amount of exchange arising within the heat exchanger. Parallel convective heat exchangers are indeed dealing with a free-boundary coupled problem for which the outlet boundary condition is not known a priori. When longitudinal conduction is taken into account, the elliptic nature of the operator to be inverted in the longitudinal direction does not permit anymore a convective boundary condition to be chosen.

In this case, a new approach has to be found and this is the main topic of this paper. We show, in the subsequent sections, how to formulate the heat exchanger outlet conditions as an unknown field coupled with inlet and outlet tubes solutions. Furthermore, we also show that the only missing outlet unknown are the uniform outlet temperatures at infinity, which can be found by inverting an explicit linear system. At this stage, it is difficult to provide more details on this new formulation, but it is progressively explained using examples of increasing complexity in Section 2.1. The adopted viewpoint is based upon the fact that stationary heat transport equations can be decomposed into generalized Graetz modes in the transverse direction, and known functions (in this paper exponential functions) in the longitudinal direction. Generalized Graetz modes are the eigenfunctions of a transverse diffusion/convection problem. They have been generalized to non-axi-symmetrical configurations recently as discussed in [21,22]. As previously discussed in [23,24] it is interesting to extend the use of generalized 2D Graetz functions for the analysis of realistic heat exchangers since they permit fast numerical solutions and provide insights on the key features of exchanges modes.

In this contribution we show how complex inlet/outlet configurations can be properly taken into account by a generalized Graetz decomposition solution. The strategy is first to compute numerically the eigenmodes which fulfill both governing equations and lateral boundary conditions, in every considered compartments: inlet, exchanger and outlet.

The resolution of two-dimensional spectral problems in each compartment provides the base for the 3-dimensional solutions in each compartment. We propose a variational formulation designed to handle the connection between the compartments of the exchanger.

It is interesting to mention, that, from the methodological point of view our approach somehow differs from standard variational methods [25,26]. Usually the space upon which the solution is formulated is not strictly restrained to the basis of admissible solutions which are generally unknown or inextinguishable from the numerical point of view. Here, since the generalized Graetz modes are only computed in two-dimensions (in the third longitudinal dimension their spatial dependence is known analytically), it is possible to first compute the admissible modes from a generalized eigenvalue problem derived from the weak-variational formulation of flux conservation equations. Then, the variational minimization is only associated with the amplitude of each element of the base. This is why the matrix to be inverted in order to find the solution is of very moderate size, since, a moderate number of modes is sufficient to obtain a good approximation.

Finally, we would like to stress that the proposed methodology equally applies to convective mass exchangers even if most of the contextual motivation and references have been mainly taken from heat transfer.

Section 1.2 provides the necessary self-consistent mathematical background and the specific notations of the considered class of problems.

Section 2 outline the general framework of the method. In Section 2.1 the variational formulation of the problem is presented whilst examples of increasing complexity are exposed in subsequent sections: Section 2.2 consider a finite domain with various inlet/outlet boundary conditions. In Section 2.3 a downstream duct is coupled to the finite domain, in Section 2.4 an upstream duct is added, and in Section 2.5 an arbitrary number of downstream/upstream ducts are considered. Finally, the proposed mode decomposition is tested in three cases for axi-symmetric domains for which an analytical mesh-free computation is performed in Section 2.6 where the spectral convergence of the method is tested.

We then proceed to the explicit and operational numerical implementation in several realistic classes of inlet/outlet configurations using a Graetz spectral decomposition in Section 3. The finite element implementation is discussed in Section 3.1, whilst the convergence in the first three axi-symmetric test cases is discussed in Section 3.2. Finally realistic exchanger geometries are discussed in Section 3.3 for imposed wall temperature at the exchanger lateral sides. A final Section 3.4 provides evidence that the results obtained with chosen $\mathcal{L}_2$ functional converges toward the same solution as another possible $\mathcal{H}_1$ functional for an increasing number of modes.

1.2. State of the art, problem formulation and notations

We consider the stationary heat transfer of temperature T inside one heat exchanger possibly connected along the longitudinal direction, to some arbitrary inlet/outlet conditions. The longitudinal direction is denoted z, whilst the two other transverse coordinates are x and y, and are also re-cast into a transverse vector $\xi = (x, y)$ for which the transverse gradient and divergence operators are denoted $\nabla = (\partial_x, \partial_y)$ and $\mathrm{div} = (\partial_x + \partial_y)$. Convection arises due to a translationally invariant velocity field $\mathbf{v} = v(\xi)\mathbf{e}_z$ independent of z which convects the fluid. For incompressible laminar flow regimes in cylindrical tubes, over a wide range of Reynolds numbers, this velocity field displays a parabolic Poiseuille shape.

In more complex ducts, e.g. hexagonal ones [27], the longitudinal velocity $v(\xi)$ is the solution of the following Poisson problem forced by the uniform longitudinal pressure gradient

$$\mathrm{div}(\nabla v) = C,$$

where $C = \partial_z p/\mu$. In what follows, we consider laminar fully developed longitudinally invariant flow profile, and we suppose that $v(\xi)$ is known. This assumption is valid for perfect liquids with constant transport properties.

The thermal conductivity k is also assumed to be isotropic and independent of z, but it can vary along the transverse direction $k = k(\xi) \in \mathbb{R}$. The geometry spans over the domain $\Omega \times I$ where Ω is a possibly complex domain in the transverse plane of ξ, and $I \subset \mathbb{R}$ is an interval along the z direction, either finite or semi-infinite. The constitutive equation for the convection/diffusion problem reads

$$\mathrm{div}(k\nabla T) + k\partial_z^2 T = v\partial_z T \quad \text{on } \Omega \times I. \tag{1}$$

General boundary conditions are imposed and detailed below. Previous contributions [21,22] have shown that in the case of Dirichlet lateral boundary conditions the solutions to Eq. (1) fulfill the following form $T = T_\lambda(\xi)\exp(\lambda z)$. This leads to the following definition for the generalized Graetz modes.

Definition Generalized Graetz modes. We consider the following problem, either for a Dirichlet or a Neumann boundary condition: find $\lambda \in \mathbb{R}$ and $T_\lambda \in L^2(\Omega)$ solutions to:

$$\mathrm{div}(k\nabla T_\lambda) + k\lambda^2 T_\lambda = v\lambda T_\lambda \quad \text{on } \Omega,$$
$$T_\lambda(\xi)_{|\partial\Omega} = 0 \quad \text{or} \quad k\nabla T_\lambda(\xi)_{|\partial\Omega} \cdot \mathbf{n} = 0.$$

This problem has the form of a generalized eigenproblem. The solutions λ therefore will be called eigenvalues. They form a spectrum Λ whose definition of course depends on the chosen Dirichlet or Neumann boundary condition. The associated eigenfunctions $(T_\lambda)_{\lambda\in\Lambda}$ are the generalized Graetz modes, also depending on the chosen boundary condition.

The mathematical properties of the generalized Graetz modes have been studied in [21–23]. Generalized Graetz modes have been first used to solve problem (1) on infinite domains in [21]. The use of generalized Graetz modes for finite and semi-infinite domains was then considered in [22]. Extensions to general lateral boundary conditions are presented in [23].

The spectrum Λ decomposes into a double sequence of positive and negative eigenvalues $\Lambda = (\lambda_n)_{n\in\mathbb{Z}^\star}$,

$$-\infty \xleftarrow[n\to+\infty]{} \lambda_n \leqslant \cdots \leqslant \lambda_1 < 0 < \lambda_{-1} \leqslant \cdots \leqslant \lambda_{-n} \xrightarrow[n\to+\infty]{} +\infty.$$

In the Neumann case with total flux $\int_\Omega v\,dx = 0$, $\lambda_0 = 0$ also is an eigenvalue with associated Graetz mode $T_0 = 1$ the constant function.

Negative eigenvalues are called downstream (they decay for $z \to +\infty$) and positive ones, upstream (they decay for $z \to -\infty$), so as the corresponding Graetz modes. In order to clearly distinguish downstream from upstream modes we define in the following

$$\forall n \in \mathbb{N}^\star, \quad T_n^+ = T_n,\ \lambda_n^+ = \lambda_n < 0 \quad \text{(downstream modes)}$$
$$T_n^- = T_{-n},\ \lambda_n^- = \lambda_{-n} > 0 \quad \text{(upstream modes)}$$

The purpose of this contribution is to demonstrate how to use the generalized Graetz modes when applying versatile inlet/outlet conditions to this heat exchanger. What we mean by versatile conditions is a mixture of Dirichlet, Neumann or Robin conditions applied at the entrance front and/or the output side of the heat exchanger. But versatile also covers couplings between the entrance and/or the output with semi-infinite tubular inlet/outlet. Such situations are relevant for applications as illustrated in [1]. A general example of configuration studied here is displayed on Fig. 1.

For the sake of simplicity since we concentrate here on inlet/outlet conditions, the analysis and results presented in this paper are restricted to outer lateral Dirichlet boundary conditions, so that for heat exchangers of longitudinal extent $(0, L)$ as in [16,6],

$$T = 0 \quad \text{on } \partial\Omega^0 \times (0, L), \tag{2}$$

along the exchanger. The presented approach is amenable to more complex situations for the applied lateral conditions. General lateral boundary conditions of Dirichlet or Neumann type can be considered following the results in [23]. Even

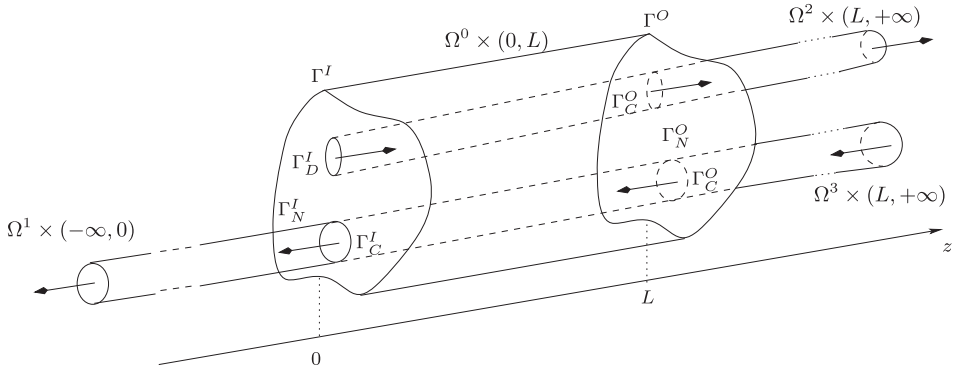

Fig. 1. Example of configuration useful for illustrating the notations associated with the domain and boundary conditions. A heat exchanger in the region $\Omega^0 \times (0, L)$ is coupled with three semi-infinite tubes. One inlet tube $\Omega^1 \times (-\infty, 0)$ that has for interface $\Gamma^I_C = \Omega^1 \times \{0\}$. Two outlet tubes $\Omega^{2,3} \times (L, +\infty)$ that have for interface $\Gamma^O_C = \Omega^2 \times \{L\} \cup \Omega^3 \times \{L\}$. In this example we moreover have $\Omega^1 = \Omega^3$. Coupling conditions (4) are imposed at the interface Γ_C. The temperature is prescribed (Dirichlet) on Γ^I_D, modeling a hot fluid injection, whereas a zero flux is imposed on $\Gamma^I_N = \Omega^0 \setminus \Omega^1 \times \{0\}$ and $\Gamma^O_N = \Omega^0 \times \{L\} \setminus \Gamma^0_C$ (homogeneous Neumann) modeling an adiabatic condition on the solid sides of the heat exchanger.

if Neumann type lateral boundary conditions might be more physically relevant to exchangers, it nevertheless provides unnecessary complexity in the presented method at this stage, and we prefer to leave this extension for future investigations.

The subscripts I and O will be used in the sequel for *Inlet* and *Outlet* respectively. The heat exchanger has for inlet $\Gamma^I = \Omega^0 \times \{0\}$ and for outlet $\Gamma^O = \Omega^0 \times \{L\}$. The total inlet/outlet domain is $\Gamma = \Gamma^I \cup \Gamma^O$. The input front and output side are partitioned into four different subsets, depending on the type of boundary conditions:

$$\Gamma^{I,O} = \Gamma^{I,O}_D \cup \Gamma^{I,O}_N \cup \Gamma^{I,O}_R \cup \Gamma^{I,O}_C.$$

It is interesting to mention that the velocity is non-zero only in $\Gamma^{I,O}_C$ because it is zero only on the solid interface $\Omega^0 \setminus \bigcup_{k>0} \Omega^k$. Furthermore in each connected component of $\Gamma^{I,O}$, the velocity field has to keep the same direction. One will impose respectively Dirichlet, Neumann or Robin boundary conditions on sub-domains D, N and R,

$$\begin{aligned} T(\xi) &= f(\xi) \quad \text{on } \Gamma_D, \\ \partial_z T(\xi) &= g(\xi) \quad \text{on } \Gamma_N, \\ \partial_z T(\xi) + \alpha(\xi) T(\xi) &= h(\xi) \quad \text{on } \Gamma_R. \end{aligned} \tag{3}$$

The sub-domain Γ_C is dedicated to the coupling interfaces between the heat exchanger and semi-infinite tubes. More precisely we consider a collection of semi-infinite tubes $\Omega^k \times I^k$ with $\Omega^k \subset \Omega^0$. They are coupled with the heat exchanger $\Omega^0 \times (0, L)$ either at the inlet, in which case $I^k = (-\infty, 0)$, or at the outlet, in which case $I^k = (L, +\infty)$. An example of such complex configuration is described in Fig. 1 with three Inlet/Outlet tubes.

On the interface Γ_C the continuity of fluxes and temperature is imposed,

$$\begin{aligned} T_{\text{left}} &= T_{\text{right}} \quad \text{on } \Gamma_C, \\ \partial_z T_{\text{left}} &= \partial_z T_{\text{right}} \quad \text{on } \Gamma_C. \end{aligned} \tag{4}$$

More precisely, we will get at the inlet Γ^I_C, at $z = 0$,

$$T_{\text{left}} = T\left(\xi, 0^-\right), \qquad T_{\text{right}} = T\left(\xi, 0^+\right),$$

whereas at the outlet Γ^O_C, at $z = L$,

$$T_{\text{left}} = T\left(\xi, L^-\right), \qquad T_{\text{right}} = T\left(\xi, L^+\right).$$

Still for the sake of simplicity, we assume a homogeneous Neumann lateral boundary condition on each semi-infinite tube,

$$k \nabla T \cdot \mathbf{n} = 0 \quad \text{on } \partial\Omega^{1,2,3} \times I^{1,2,3}, \tag{5}$$

A Dirichlet boundary condition could also be considered, as well as a mixture of Dirichlet/Neumann conditions depending on the considered semi-infinite tube.

An important note relative to condition (5) is the following. Consider an inlet tube $\Omega^k \times (-\infty, 0)$ in which the fluid flows towards the $z > 0$ direction and thus enters the heat exchanger at the interface. In this case the temperature $T^{-\infty}$ as $z \to -\infty$ is a data of the problem and will be imposed. Consider now the same inlet tube $\Omega^k \times (-\infty, 0)$ where the fluid is now assumed to flow in the $z < 0$ direction and so leaves the heat exchanger at the interface. In this case the temperature $T^{-\infty}$ is an unknown of the problem that one wishes to recover. The same considerations hold for the temperature $T^{+\infty}$ as $z \to +\infty$ in outlet tubes but reversed.

2. Resolution method

2.1. Variational formulation

We want to solve problem (1) for the configuration described in Section 1.2, with specified inlet/outlet conditions (3) and continuous coupling with semi-infinite domains (4).

In standard finite elements or spectral methods, one would minimize a cost function whose derivative is the partial differential equation of interest (1) on a space that fulfills the boundary conditions. On the contrary, in our problem The space of solutions of (1) is at our disposal thanks to the Graetz modes decomposition. We propose to define a cost function that measures the discrepancy with the desired boundary conditions. More precisely, we introduce the functional $J_{\mathcal{L}_2}$ as

$$\begin{aligned} J_{\mathcal{L}_2}(T) = &\int_{\Gamma_D} |T - f|^2 \, ds + \int_{\Gamma_N} |\partial_z T - g|^2 \, ds \\ &+ \int_{\Gamma_R} |\partial_z T + \alpha T - h|^2 \, ds + \int_{\Gamma_C} |T_{\text{left}} - T_{\text{right}}|^2 \, ds \\ &+ \int_{\Gamma_C} |\partial_z T_{\text{left}} - \partial_z T_{\text{right}}|^2 \, ds \end{aligned} \tag{6}$$

and minimize $J_{\mathcal{L}_2}$ over the set of solutions of (1), hereafter denoted V. $\mathcal{L}_2$ refers to the $\mathcal{L}_2$ norm which is hereby chosen in (6) for the temperature and normal gradient $\mathcal{L}_2$ difference between the inlet and the outlet compartments. Other choices are possible but, for simplicity in the exposition of the method implementation, we concentrate on this first choice in the following. We will nevertheless examine another choice in Section 3.4, for propounding more mathematically sound functional. We will illustrate, in some examples, that the results obtained using another functional differ, but the difference between the obtained solutions numerically converges as the mode number increases.

Here, the space V is known using the Graetz modes, as detailed in the following. Consider a solution T to (1), (2), (3), (4) and (5), then it clearly satisfies $T \in V$ and $J_{\mathcal{L}_2}(T) = 0$. Reciprocally it is also true and the two problems are equivalent. Moreover when $J_{\mathcal{L}_2}(T) = 0$ then T also is a minimizer of $J_{\mathcal{L}_2}$ over V. The continuous problem: find a solution T to (1), (2), (3), (4) and (5) is equivalent to the following minimization problem: find $T \in V$ so that $J_{\mathcal{L}_2}(T) = \min_{S \in V} J_{\mathcal{L}_2}(S)$ and $J_{\mathcal{L}_2}(T) = 0$. We do not address the question of existence and uniqueness of such solution, we numerically solve the problem of minimization.

Our numerical approach consists in approximating the space V by a finite dimensional space V_N of dimension N, namely the one obtained by extracting the first generalized Graetz modes in Definition 1.2 and to minimize $J_{\mathcal{L}_2}$ on V_N. Once V_N is defined, we minimize $J_{\mathcal{L}_2}$ on V_N. Since $J_{\mathcal{L}_2}$ is quadratic, upon choosing a finite dimensional space V_N basis, the problem may be re-cast into the inversion of the following linear problem:

Finite dimensional problem Let $(e_k)_{k=1\dots N}$ be a basis of the space V_N, decompose,

$$J_{\mathcal{L}_2}(T) = m(T, T) + b(T) + c,$$

with m bilinear symmetric, b linear and c a constant. Let $\mathbf{M}_{\mathcal{L}_2} \in \mathbb{R}^{N \times N}$ and $\mathbf{b} \in \mathbb{R}^N$ defined as $\mathbf{M}_{\mathcal{L}_2\, ij} = m(e_i, e_j)$ and $\mathbf{b}_i = b(e_i)$. Find $\mathbf{x} \in \mathbb{R}^N$ solution of,

$$\mathbf{M}_{\mathcal{L}_2} \mathbf{x} = \mathbf{b}. \tag{7}$$

The solution $\mathbf{x}$ of (7), yields $T_N = \sum_{j=1}^{p} x_j e_j$ a minimum point of $J_{\mathcal{L}_2}$ over V_N. The function T_N is then our approximation of the minimum point of $J_{\mathcal{L}_2}$ over V. Also note that with the definition (6), the matrix $\mathbf{M}_{\mathcal{L}_2}$ is symmetric positive.

The linear system (7) which involves the matrix $\mathbf{M}_{\mathcal{L}_2}$ is expected to be of very modest size, typically $N < 100$. This is because the essential information is already stored within the generalized Graetz modes. Hence, formulation (7) is the main result of this contribution since the proposed spectral approach drastically reduces the numerical complexity of the heat exchanger modes decomposition [28]. In the following sections, we consider different geometries sorted in increasing order of complexity.

For each configuration, we provide the case-specific functional spaces, and the detailed formulation of matrix $\mathbf{M}_{\mathcal{L}_2}$ and vector $\mathbf{b}$. In the following matrix and vectors will be indexed by I for inlet – resp. O for outlet – when they are related to the imposed Inlet – resp. Outlet – conditions. Furthermore, since different compartments are coupled the corresponding matrix, vectors and domains are associated with upper index related to the compartment number as previously introduced: 0 for the heat exchanger compartment, 1 and 2 to upstream/downstream tubes compartments, as illustrated for Ω^0, Ω^1 and Ω^2 in Figs. 2, 3 and 5.

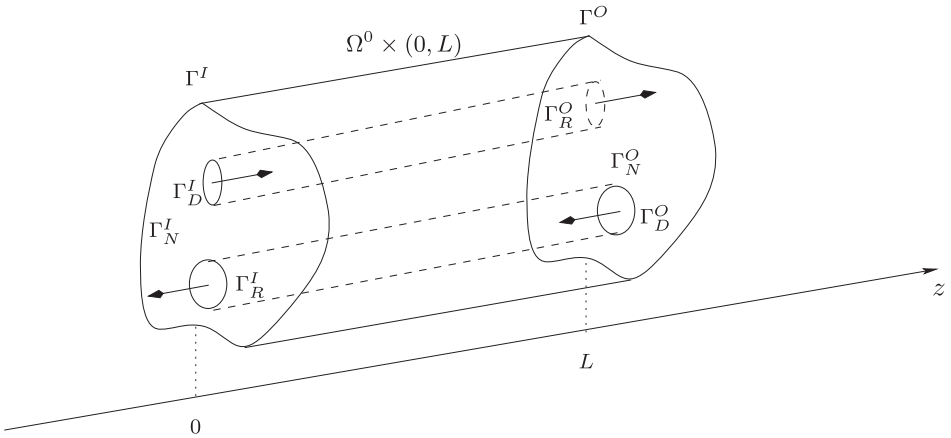

Fig. 2. Example of heat exchanger configuration with specified inlet/outlet conditions studied in Section 2.2. In this example, we consider Neumann adiabatic insulate conditions at inlet $\Gamma_N^{I,O}$ (solid part), prescribed Dirichlet on $\Gamma_D^{I,O}$ (fluid injection) and Robin boundary conditions on $\Gamma_R^{I,O}$ (fluid outlet).

2.2. *Specified inlet/outlet condition for a single heat exchanger*

We consider in this section the problem (1)–(2) on the heat exchanger $\Omega^0 \times (0, L)$ together with the specified inlet/outlet conditions (3). An example of such a configuration is displayed in Fig. 2.

Applying the ideas of Section 2.1 and the problem of Definition 2.1, we consider V^0 the set of solutions of (1)–(2), associated with heat exchanger compartment indexed with number 0. It is given by,

$$V^0 = \left\{ T(\xi, z) = \sum_{\mathbb{N}^\star} x_n^+ T_n^+(\xi) e^{\lambda_n^+ z} + x_n^- T_n^-(\xi) e^{\lambda_n^-(z-L)} \right\}, \tag{8}$$

involving the generalized Graetz modes $T_n^\pm$ and the eigenvalues $\lambda_n^\pm$ in Definition 1.2 relatively to the domain Ω^0 and to the Dirichlet boundary condition on $\partial\Omega^0$. A precise study of the mathematical properties of V^0 is provided in [22]. The finite sub-space V_N^0 which approximates V^0 is obtained by truncating with the N^+ first downstream modes and N^- upstream modes

$$V_N^0 = \left\{ T(\xi, z) = \sum_{n=1}^{N^+} x_n^+ T_n^+(\xi) e^{\lambda_n^+ z} + \sum_{n=1}^{N^-} x_n^- T_n^-(\xi) e^{\lambda_n^-(z-L)} \right\}.$$

The dimension of V_N^0 is $N = N^+ + N^-$. A straightforward basis of V_N^0 is $(e_k^0)_{1 \leqslant k \leqslant N}$ defined as,

$$\begin{cases} e_k^0 : (\xi, z) \mapsto T_k^+(\xi) e^{\lambda_k^+ z} & \text{if } 1 \leqslant k \leqslant N^+ \\ e_{(N^+ + k)}^0 : (\xi, z) \mapsto T_k^-(\xi) e^{\lambda_k^-(z-L)} & \text{if } 1 \leqslant k \leqslant N^- \end{cases} \tag{9}$$

We recast, as stated in Definition 2.1, the minimization of $J_{\mathcal{L}_2}$ over V_N^0 into the problem $\mathbf{M}^0 x = \mathbf{b}^0$ where, again, index 0 refers to the heat exchanger compartment number (not to be confused with the outlet O). In this case the bilinear functional m of Definition 2.1 may be decomposed into the sum of two bilinear functional $m = m^I + m^O$, the form m^I (resp. m^O) taking into account the effects on the Inlet (resp. Outlet), i.e.

$$m^I(T, T) = \int_{\Gamma_D^I} T(\xi, 0)^2 + \int_{\Gamma_N^I} \partial_z T(\xi, 0)^2 + \int_{\Gamma_R^I} \big(\partial_z T(\xi, 0) + \alpha(\xi) T(\xi, 0)\big)^2,$$

$$m^O(T, T) = \int_{\Gamma_D^O} T(\xi, L)^2 + \int_{\Gamma_N^O} \partial_z T(\xi, L)^2 + \int_{\Gamma_R^O} \big(\partial_z T(\xi, L) + \alpha(\xi) T(\xi, L)\big)^2.$$

In order to compute the matrices $\mathbf{M}^I$ and $\mathbf{M}^O$, let us introduce the eight auxiliary matrix $\mathbf{K}^I_{\pm,\pm}$ and $\mathbf{K}^O_{\pm,\pm}$ whose coefficients are defined if $(a, b) \in \{-, +\}$, $c \in \{I, O\}$, $1 \leqslant i \leqslant N^a$, $1 \leqslant j \leqslant N^b$ by,

$$\mathbf{K}^c_{ab}(i, j) = \int_{\Gamma_D^c} T_i^a T_j^b + \int_{\Gamma_N^c} \lambda_i^a \lambda_j^b T_i^a T_j^b + \int_{\Gamma_R^c} \big(\lambda_i^a + \alpha\big) T_i^a \big(\lambda_j^b + \alpha\big) T_j^b.$$

Note that by definition, the matrix $\mathbf{K}^I_{+-}$ (resp. $\mathbf{K}^O_{+-}$) and $\mathbf{K}^I_{-+}$ (resp. $\mathbf{K}^O_{-+}$) are transposed of one-another, so that there are only six different matrix $\mathbf{K}^{I,O}_{\pm\pm}$ to evaluate. Then the matrix $\mathbf{M}^I$ and $\mathbf{M}^O$, which are the representation on the basis (e^0_k) of the bilinear forms m^I and m^0, are given by

$$\mathbf{M}^I = \begin{pmatrix} \mathbf{K}^I_{++} & \mathbf{K}^I_{+-}\mathbf{D}_- \\ \mathbf{D}_-\mathbf{K}^I_{+-} & \mathbf{D}_-\mathbf{K}^I_{--}\mathbf{D}_- \end{pmatrix}$$
$$\mathbf{M}^O = \begin{pmatrix} \mathbf{D}_+\mathbf{K}^O_{++}\mathbf{D}_+ & \mathbf{D}_+\mathbf{K}^O_{+-} \\ \mathbf{K}^O_{+-}\mathbf{D}_+ & \mathbf{K}^O_{--} \end{pmatrix}, \tag{10}$$

where the matrix $\mathbf{D}_\pm$ are the diagonal matrix

$$\mathbf{D}_\pm = \mathrm{Diag}\big(e^{\pm\lambda^\pm_1 L}, \dots, e^{\pm\lambda^\pm_N L}\big) \tag{11}$$

Assembling the matrix $\mathbf{M}^0 = \mathbf{M}^I + \mathbf{M}^O$ thus necessitates

- the computation of the six matrix $\mathbf{K}^{I,O}_{\pm\pm}$ of size $N^\pm \times N^\pm$,
- the assembly procedure (10).

The left-hand side $\mathbf{b}^0$ similarly decomposes into $\mathbf{b}^0 = \mathbf{b}^I + \mathbf{b}^O$, where the vectors $\mathbf{b}^I$ (resp. $\mathbf{b}^O$) take into account the effects of the Inlet (resp. Outlet) side only and represent the linear forms b^I (resp. b^O) on the basis (e^0_k) of V^0_N, given by

$$b^I(T) = \int_{\Gamma^I_D} Tf\,ds + \int_{\Gamma^I_N} \partial_z T g\,ds + \int_{\Gamma^I_R} (\partial_z T + \alpha T)h\,ds,$$
$$b^O(T) = \int_{\Gamma^O_D} Tf\,ds + \int_{\Gamma^O_N} \partial_z T g\,ds + \int_{\Gamma^O_R} (\partial_z T + \alpha T)h\,ds.$$

We introduce the auxiliary vectors $\beta^{I,O}_\pm \in \mathbb{R}^{N^\pm}$ defined as,

$$\beta^{I,O}_\pm(i) = \int_{\Gamma^{I,O}_D} T^\pm_i f\,ds + \int_{\Gamma^{I,O}_N} \lambda^\pm_i T^\pm_i g\,ds + \int_{\Gamma^{I,O}_R} \big(\lambda^\pm_i + \alpha\big)T^\pm_i h\,ds. \tag{12}$$

Finally we obtain,

$$\mathbf{b}^0 = \mathbf{b}^I + \mathbf{b}^O, \quad \text{with}$$
$$\mathbf{b}^I = \begin{vmatrix} \beta^I_+ \\ \mathbf{D}_-\beta^I_- \end{vmatrix}, \qquad \mathbf{b}^O = \begin{vmatrix} \mathbf{D}_+\beta^O_+ \\ \beta^O_- \end{vmatrix}, \tag{13}$$

where $\mathbf{D}_\pm$ are defined in (11).

2.3. Coupling between a heat exchanger and an outlet tube

In this section, we consider the heat exchanger $\Omega^0 \times (0, L)$ coupled with an outlet tube $\Omega^1 \times (L, +\infty)$. Their interface is $\Gamma^O_C = \Omega^1 \times \{L\}$. As previously mentioned, we assume that the flow in this outlet tube occurs in the $z > 0$ direction. An example of such a configuration is described in Fig. 3.

We consider two problems. Eqs. (1) (2) on the heat exchanger $\Omega^0 \times (0, L)$ on the first hand and Eqs. (1) (5) on the outlet tube $\Omega^1 \times (L, +\infty)$ on the second hand. These two problems are coupled with the coupling conditions (4) on Γ^O_C, and the coupled system is closed considering prescribed boundary conditions (3) on Γ^I and on $\Gamma^O - \Gamma^O_C$.

There are two Graetz problems in this setting. One is set on Ω^0 for a homogeneous Dirichlet boundary condition on $\partial\Omega^0$ relatively to the heat exchanger. The second is set on Ω^1 for a homogeneous Neumann boundary condition on $\partial\Omega^1$ relatively to the outlet tube. We denote $(T^\pm_n, \lambda^\pm_n)$ the Graetz modes defined for the heat exchanger and $(t^\pm_n, \mu^\pm_n)$ the Graetz modes defined for the outlet tube. The space of solutions of (1) (2) in $\Omega^0 \times (0, L)$ is exactly V^0, defined in (8) in the previous section. The space of solutions of (1) (5) in $\Omega^1 \times (L, +\infty)$ is V^1 given by:

$$V^1 = \left\{ T(\xi, z) = x_0 + \sum_{\mathbb{N}^\star} x_n t^+_n(\xi) e^{\mu^+_n (z-L)} \right\}. \tag{14}$$

The upstream Graetz modes t^-_n associated to eigenvalues $\mu^-_n > 0$ do not contribute to the space V^1 since they diverge at $z = +\infty$. Moreover, the definition of V^1 involves a constant x_0 which is the uniform temperature value at infinity

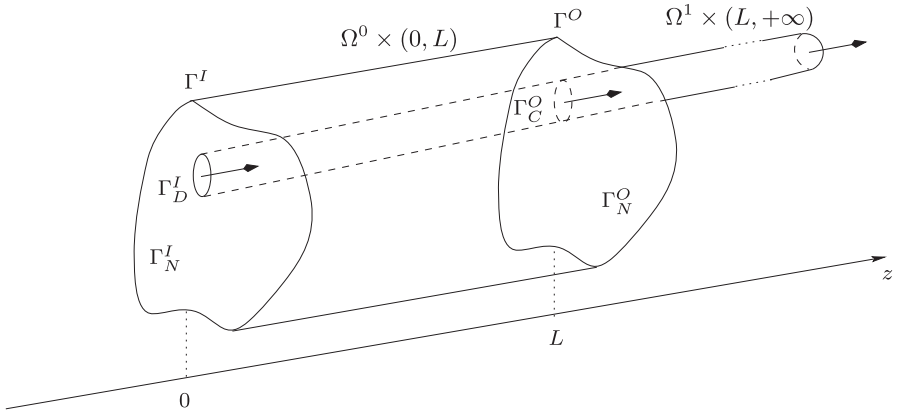

Fig. 3. Exchanger coupled with an outlet tube of section Ω^1. An upward Dirichlet condition is prescribed on Γ^I_D, an upward and backward Neumann condition is prescribed on $\Gamma^{I,O}_N$ and coupling conditions are prescribed $\Gamma^O_C = \Omega^1 \times \{L\}$ on the interface with the outlet tube. The temperature $T^{+\infty}$ at infinity is an unknown of the problem.

$x_0 = T^{+\infty}$. This temperature at infinity is an unknown of the problem. In order to simplify notations, we set $t^+_0 = 1$ the constant function and $\mu^+_0 = 0$.

The space of solutions for the complete problem is obviously the set of T whose restriction on $z \in (0, L)$ belongs to V^0 and whose restriction on $z \geqslant L$ belongs to V^1. If $0 \leqslant z \leqslant L$ this set V is given by

$$V = \left\{ T(\xi, z) = \sum_{\mathbb{N}^\star} x^+_n T^+_n(\xi) e^{\lambda^+_n z} + \sum_{\mathbb{N}^\star} x^-_n T^-_n(\xi) e^{\lambda^-_n (z-L)} \right\},$$

whilst otherwise if $L \leqslant z$

$$V = \left\{ \sum_{\mathbb{N}} x_n t^+_n(\xi) e^{\mu^+_n (z-L)} \right\}.$$

The approximation space V_N is built similarly as in the previous section, we shall keep N^+ (resp. N^-) upward (resp. downward) modes of the heat exchanger and $N^O + 1$ modes of the outlet tube. The space V_N of dimension $N = N^+ + N^- + N^O + 1$ admits a basis $(e^1_k)_{1 \leqslant k \leqslant N}$ which is built similarly as for space V^0_N in (9). This basis is first built by extending the basis functions e^0_k by zero outside the interval $z \in (0, L)$ and then by adding vectors e_k for $N^+ + N^- < k \leqslant N$ in order to approximate the space V^1. Namely we define $V_N = \mathrm{Span}(e^1_k,\ 1 \leqslant k \leqslant N)$ with,

$$\begin{aligned} &\text{for } 1 \leqslant k \leqslant N^+ + N^-, \quad e^1_k(\xi, z) = \begin{cases} e^0_k(\xi, z) & \text{if } 0 \leqslant z \leqslant L \\ 0 & \text{if } z > L \end{cases}, \\ &\text{for } 0 \leqslant k \leqslant N^O, \quad e^1_{k'}(\xi, z) = \begin{cases} 0 & \text{if } 0 \leqslant z \leqslant L \\ t^+_k(\xi) e^{\mu^+_k (z-L)} & \text{if } z > L \end{cases}, \end{aligned} \tag{15}$$

where $k' = k + N^- + N^+ + 1$. As previously, we recast the minimization of $J_{\mathcal{L}_2}$ over V_N into the problem $\mathbf{M}^1 x = \mathbf{b}^1$. The matrix $\mathbf{M}^1$ to invert is decomposed into,

$$\mathbf{M}^1 = \begin{bmatrix} \mathbf{M}^0 & 0 \\ 0 & 0 \end{bmatrix} + \mathbf{M}^O_C,$$

where $\mathbf{M}^0 = \mathbf{M}^I + \mathbf{M}^O$ is the square matrix of size $N^+ + N^-$ defined in (10) and is associated to the prescribed conditions (3) on Γ. The matrix $\mathbf{M}^O_C$ is related with the couplings at the interface Γ^O_C between the exchanger and the outlet tube whose associated bilinear form is given by

$$m^O_C(T, T) = \int_{\Gamma^O_C} |T_{|\text{left}} - T_{|\text{right}}|^2 + |\partial_z T_{|\text{left}} - \partial_z T_{|\text{right}}|^2 \, ds.$$

The assembling of $\mathbf{M}^O_C$ necessitates the evaluation of three classes of matrix $\mathbf{Q}_{\pm\pm}$, $\mathbf{R}_{\pm+}$ and $\mathbf{S}+$ whose coefficients are given by, for $(a, b) \in \{-, +\}^2$,

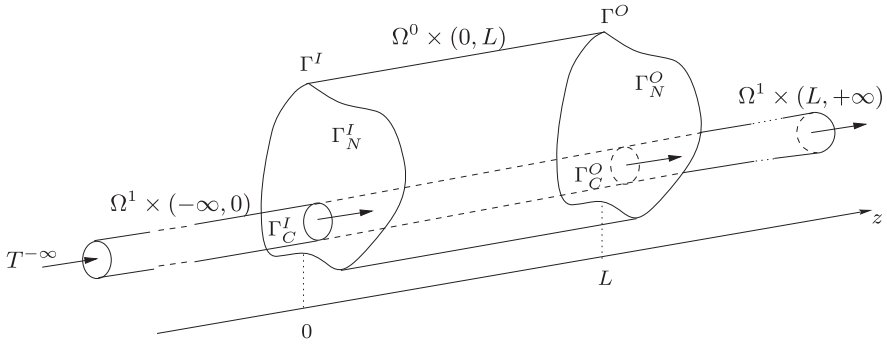

Fig. 4. Exchanger coupling with one inlet and one outlet tubes and with $\Omega^1 = \Omega^2$ studied in Section 2.4. On this example illustration, an adiabatic frontier $\Gamma^{I,O}_N$ is added. The temperatures at infinity are homogeneous and equals to $T^{\pm\infty}$, $T^{-\infty}$ is a data and $T^{+\infty}$ is an unknown.

$$\mathbf{Q}_{ab}(i,j) = \left(1 + \lambda_i^a \lambda_j^b\right) \int_{\Omega_1} T_i^a T_j^b \, ds, \quad \text{for } 1 \leqslant i \leqslant N^a,\ 1 \leqslant j \leqslant N^b,$$

$$\mathbf{R}_{a+}(i,j) = \left(1 + \lambda_i^a \mu_j^+\right) \int_{\Omega_1} T_i^a t_j^+ \, ds, \quad \text{for } 1 \leqslant i \leqslant N^a \text{ and } 0 \leqslant j \leqslant N^O,$$

$$\mathbf{S}_+(i,j) = \left(1 + \mu_i^+ \mu_j^+\right) \int_{\Omega_1} t_i^+ t_j^+ \, ds, \quad \text{for } 0 \leqslant i, j \leqslant N^O. \tag{16}$$

Note that $\mathbf{Q}_{+-} = {}^{\mathbf{T}}\mathbf{Q}_{-+}$ and that $\mathbf{Q}_{++}$ are matrix of size $N^\pm \times N^\pm$, $\mathbf{R}_\pm$ are matrix of size $N^\pm \times (N^O + 1)$ and finally that the matrix $\mathbf{S}_+$ is of size $(N^O + 1) \times (N^O + 1)$.

The matrix $\mathbf{M}^O_C$ is then defined as,

$$\mathbf{M}^O_C = \begin{bmatrix} \mathbf{M}_+ & \mathbf{C}_+ \\ {}^{\mathbf{T}}\mathbf{C}_+ & \mathbf{S}_+ \end{bmatrix},$$

where $\mathbf{M}_+$ is a square matrix of size $N^+ + N^-$, $\mathbf{C}_+$ is of size $(N^+ + N^-) \times (N^O + 1)$ and $\mathbf{S}_+$ is square of size $(N^O + 1) \times (N^O + 1)$, they are given by the following formula

$$\mathbf{M}_+ = \begin{bmatrix} \mathbf{D}_+\mathbf{Q}_{++}\mathbf{D}_+ & \mathbf{D}_+\mathbf{Q}_{+-} \\ \mathbf{Q}_{+-}\mathbf{D}_+ & \mathbf{Q}_{--} \end{bmatrix} \quad \& \quad \mathbf{C}_+ = \begin{bmatrix} -\mathbf{R}_{++} \\ -\mathbf{R}_{-+} \end{bmatrix}, \tag{17}$$

where $\mathbf{D}_+$ is the diagonal matrix defined in (11). Hence, matrix $\mathbf{M}^1$ finally reads,

$$\mathbf{M}^1 = \begin{bmatrix} \mathbf{M}^0 & \mathbf{0} \\ \mathbf{0} & \mathbf{0} \end{bmatrix} + \begin{bmatrix} \mathbf{M}_+ & \mathbf{C}_+ \\ {}^{\mathbf{T}}\mathbf{C}_+ & \mathbf{S}_+ \end{bmatrix}. \tag{18}$$

The assembling of the left-hand-size is not modified by the coupling of additional constraint, so that it reads $\mathbf{b}^1 = (\mathbf{b}^0, \mathbf{0})$, where $\mathbf{b}^0$ is the vector of size $N^+ + N^-$ defined in (13) and is associated with the prescribed Dirichlet and Neumann boundary conditions on Γ.

2.4. Coupling between a heat exchanger, an inlet and an outlet tube

In addition to the previous considered configuration, we now add an inlet tube $\Omega^1 \times (-\infty, 0)$. As in the previous section, we assume that the flow in this inlet/outlet tubes occurs in the $z > 0$ direction.

We now are dealing with three different problems: problem (1) (2) on the heat exchanger $\Omega^0 \times (0, L)$, problem (1) (5) on the inlet tube $\Omega^1 \times (-\infty, 0)$ and problem (1) (5) on the outlet tube $\Omega^1 \times (L, +\infty)$. These three problems are considered together with,

- coupling conditions (4) at the inlet interface $\Gamma^I_C = \Omega^1 \times \{0\}$ and outlet interface $\Gamma^O_C = \Omega^1 \times \{L\}$,
- prescribed conditions (3) on the remaining parts of Γ^I and Γ^O,
- at $z = -\infty$, the temperature $T^{-\infty}$ independent of ξ is imposed as a constraint of the problem, whereas at $z = +\infty$ the temperature $T^{+\infty}$ is unknown and one free parameter of the problem.

An example of such a configuration is displayed on Fig. 4.

The space of solutions for (1) (2) on $\Omega^0 \times (0, L)$ is V^0 defined in (8). The space of solutions for (1) (5) on $\Omega^1 \times (L, +\infty)$ is V^1 defined in (14). Eventually, the set of solutions for (1) (5) on $\Omega^1 \times (-\infty, 0)$ is V^2 given by,

$$V^2 = \left\{ T(\xi, z) = T^{-\infty} + \sum_{\mathbb{N}^\star} x_n t_n^-(\xi) e^{\mu_n^- z} \right\}, \tag{19}$$

where $(t_n^-, \mu_n^-)_n$ are the downstream generalized Graetz modes associated to the domain Ω^1 with Neumann boundary condition. The solution of this coupled problem is searched for in the set V,

$$V = \left\{ T,\ T_{|\Omega^0 \times (0,L)} \in V^0,\ T_{|\Omega^1 \times [L, +\infty[} \in V^1 \text{ and } T_{|\Omega^1 \times]-\infty, 0]} \in V^2 \right\}.$$

Keeping our approximation consistent with the one of the previous sections leads to building a vector space V_N of dimension $N = N^+ + N^- + (N^O + 1) + N^I$, with basis $(e_k^2)_{1 \leqslant k \leqslant N}$ constructed as previously:

$$\text{for } 1 \leqslant k < N - N^1, \quad e_k^2(\xi, z) = \begin{cases} e_k^1(\xi, z) & \text{if } z > 0 \\ 0 & \text{if } z < 0 \end{cases},$$

$$\text{for } 1 \leqslant k \leqslant N^I, \quad e_{k+N-N^I}^2(\xi, z) = \begin{cases} 0 & \text{if } z > 0 \\ t_k^-(\xi) e^{\mu_k^- z} & \text{if } z < 0 \end{cases},$$

using the basis function e_k^1 defined in (15). The approximation space is then the affine space,

$$V_N = \left\{ T \in T^{+\infty} \chi_{z<0} \oplus \text{Span}(e_k,\ 1 \leqslant k \leqslant N) \right\}$$

The matrix $\mathbf{M}_{\mathcal{L}_2}$ of the linear system (7) decomposes in the following blocks,

$$\mathbf{M}_{\mathcal{L}_2} = \begin{bmatrix} \mathbf{M}^1 & \mathbf{0} \\ \mathbf{0} & \mathbf{0} + \mathbf{M}_C^I \end{bmatrix},$$

where the matrix $\mathbf{M}^1$ on the right-hand-side, defined in (18), is associated with prescribed conditions of functional $J_{\mathcal{L}_2}$ and downstream couplings. The second matrix $\mathbf{M}_C^I$ on the right-hand-side is associated with the inlet coupling, and is precisely given by the bilinear form m_C^I defined as

$$m_C^I(T) = \int_{\Gamma_C^I \times \{0\}} |T_{|\text{left}} - T_{|\text{right}}|^2 + |\partial_z T_{|\text{left}} - \partial_z T_{|\text{right}}|^2 \, ds.$$

Calculations show that the matrix $\mathbf{M}_C^I$ has a similar definition than the one of $\mathbf{M}_C^O$, that is it admits the following block-decomposition

$$\mathbf{M}_C^I = \begin{bmatrix} \mathbf{M}_- & \mathbf{0} & \mathbf{C}_- \\ \mathbf{0} & \mathbf{0} & \mathbf{0} \\ {}^T\mathbf{C}_- & \mathbf{0} & \mathbf{S}_- \end{bmatrix},$$

where the square matrix $\mathbf{M}_-$ is of size $N^+ + N^-$, where the matrix $\mathbf{C}_-$ is size $(N^+ + N^-) \times N^I$, and where those matrix are defined as

$$\mathbf{M}_- = \begin{bmatrix} \mathbf{Q}_{++} & \mathbf{Q}_{+-}\mathbf{D}_- \\ \mathbf{D}_-\mathbf{Q}_{+-} & \mathbf{D}_-\mathbf{Q}_{--}\mathbf{D}_- \end{bmatrix} \quad \& \quad \mathbf{C}_- = \begin{bmatrix} -\mathbf{R}_{+-} \\ -\mathbf{R}_{--} \end{bmatrix}, \tag{20}$$

where $\mathbf{D}_-$ is defined in (11), where the matrix $\mathbf{Q}_{\pm\pm}$ are defined in (16), and where the formula for $\mathbf{R}_{\pm-}$ (resp. $\mathbf{S}_-$) are obtained from the formula for $\mathbf{R}_{\pm+}$ (resp. $\mathbf{S}_+$) in (16) upon replacing t^+ by t^-. Finally the matrix $\mathbf{M}_{\mathcal{L}_2}$ reads

$$\mathbf{M}_{\mathcal{L}_2} = \begin{bmatrix} \mathbf{M}^1 & \mathbf{0} & \mathbf{0} \\ \mathbf{0} & \mathbf{0} & \mathbf{0} \\ \mathbf{0} & \mathbf{0} & \mathbf{0} \end{bmatrix} + \begin{bmatrix} \mathbf{M}_+ & \mathbf{C}_+ & \mathbf{0} \\ {}^T\mathbf{C}_+ & \mathbf{S}_+ & \mathbf{0} \\ \mathbf{0} & \mathbf{0} & \mathbf{0} \end{bmatrix} + \begin{bmatrix} \mathbf{M}_- & \mathbf{0} & \mathbf{C}_- \\ \mathbf{0} & \mathbf{0} & \mathbf{0} \\ {}^T\mathbf{C}_- & \mathbf{0} & \mathbf{S}_- \end{bmatrix},$$

The left-hand-side $\mathbf{b}$ of (7) $\mathbf{b}$ is modified from the previous case due to the presence of the source term $T^{-\infty}$ (imposed temperature at $z = -\infty$),

$$\mathbf{b} = \begin{vmatrix} \mathbf{b}^0 \\ 0 \\ \mathbf{b}^{-\infty} \end{vmatrix},$$

where $\mathbf{b}^{-\infty}$ is a N^I dimensional vector whose components are $\mathbf{b}^{-\infty}(i) = T^{-\infty} \int_{\Omega^1} t_i^-(\xi) \, ds$, and with $\mathbf{b}^0$ defined by (13).

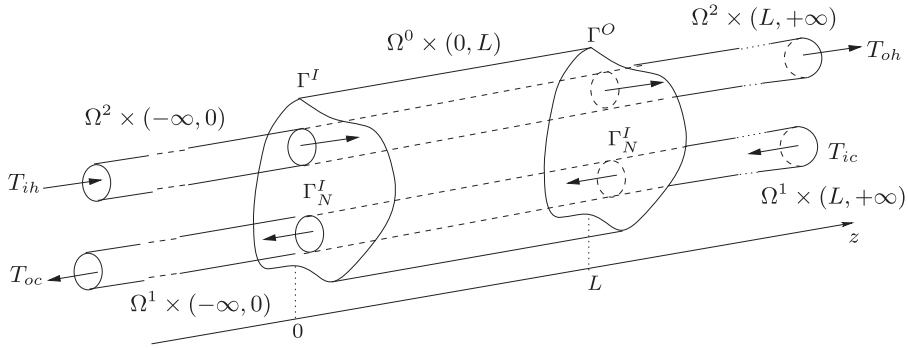

Fig. 5. Example of a finite domain heat exchanger coupled with two inlet/outlet tubes. The first tube with section Ω^1 models an injection of hot fluid with input temperature T_{ih} at $z = +\infty$. The second tube with section Ω^2 models an injection of cold fluid with input temperature T_{ic} at $z = -\infty$. The input-hot and input-cold fluid temperatures T_{ih} and T_{ic} are imposed data. After passing through the heat exchanger $\Omega^0 \times (0, L)$ with prescribed wall temperature $T_w = 0$, the hot (resp. cold) fluid reaches the output-hot temperature T_{oh} (resp. output-cold T_{oc}) at $z = -\infty$ (resp. $z = +\infty$). The output-hot and output-cold fluid temperatures T_{oh} and T_{oc} are problem unknowns. The two inlet tubes $\Omega^{1,2} \times (-\infty, 0)$ are coupled with the heat exchanger with conditions (4) on $\Gamma^I_C = (\Omega^1 \cup \Omega^2) \times \{0\}$. Similarly the two outlet tubes $\Omega^{1,2} \times (L, +\infty)$ are coupled with the heat exchanger with conditions (4) on $\Gamma^O_C = (\Omega^1 \cup \Omega^2) \times \{L\}$. The solid parts Γ^I_N and Γ^I_N of the inlet/outlet are associated with an adiabatic conditions. This configuration is numerically investigated in Section 3.3.1.

2.5. General case

In the light of the previous cases it is possible to build the linear system associated with the solution of the general case (7) for a heat exchanger $\Omega^0 \times (0, L)$ coupled with an arbitrary number of inlet and outlet tubes. One example is illustrated in Fig. 5.

The heat exchanger temperature is searched in the space define by (8). In each tube, the temperature is searched via,

- (14) for an inlet tube or,
- (19) for an outlet one.

We specify that, in each tube, the first constant term in decompositions (14), (19) has to be treated

- either as an unknown in case the fluid leaves the heat exchanger and enters the tube at their interface (unknown temperature at the duct end),
- or conversely as a data in case the fluid enters the heat exchanger and thus leaves the tube at their interface (prescribed temperature at the duct end).

Considering modes $t_i^{\pm}(\xi)$, $\mu_i^{\pm}$ for each considered inlet/outlet tubes, the matrix M to invert reads,

$$\mathbf{M}_{\mathcal{L}_2} = \begin{bmatrix} \mathbf{M}^0 + \mathbf{M}^1 + \cdots + \mathbf{M}^p & \mathbf{C}_1 & \cdots & \mathbf{C}_p \\ {}^T\mathbf{C}_1 & \mathbf{S}_1 & & \\ \vdots & & \ddots & \\ {}^T\mathbf{C}_p & & & \mathbf{S}_p \end{bmatrix}.$$

The block decomposition of $M_{\mathcal{L}_2}$ involves,

- the matrix $\mathbf{M}^0 = \mathbf{M}^I + \mathbf{M}^O$ in (10),
- the matrix $\mathbf{M}^i$ are either $\mathbf{M}_+$ in (17) or $\mathbf{M}_-$ in (20) depending on the ith tube to be an inlet or an outlet,
- similarly the matrix $\mathbf{C}_i$ (resp. matrix $\mathbf{S}_i$) is either $\mathbf{C}_+$ (resp $\mathbf{S}_+$) in (17) or $\mathbf{C}_-$ (resp. $\mathbf{S}_-$) in (20) depending on the ith tube to be an inlet or an outlet.

2.6. Convergence with number of modes

In this section we discuss the numerical convergence of the functional minimization described in Section 2.1 with the considered number N of generalized Graetz modes. The aim of this section is to specifically analyze mode truncation errors independently of mesh discretization errors. For this, we consider an axi-symmetric configuration with cylindrical tubes. In this case, a formal analytical computation of modes $T_{\pm i}$ and their related eigenvalue $\lambda_{\pm i}$ is available following the method described in [29].

We consider three test cases based on a the same geometry made of two concentric axi-symmetric cylinders. More precisely, for each case, the inlet/outlet tubes section Ω^1 is the unit circle that is embedded in the heat exchanger section Ω^0 equal to the circle of radius $R = 2$ and with same center C. The exchanger length is set to $L = 3R = 6$. The flow has the

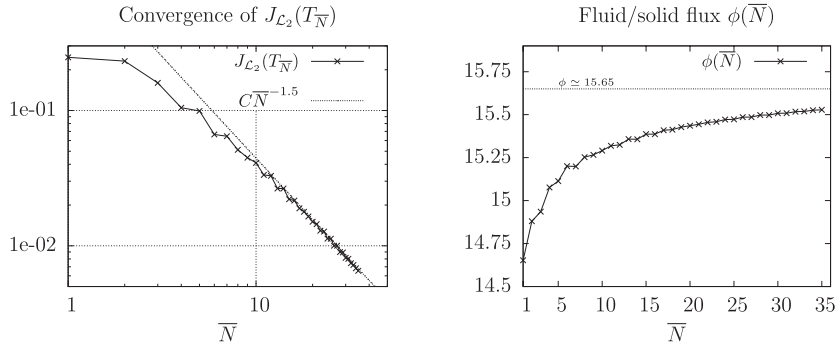

Fig. 6. Test case 1: convergence of $J_{\mathcal{L}_2}(T_N)$ toward zero using log–log coordinated (left) and the predicted fluid/solid flux convergence $\phi(N)$ (right) versus N_{modes}.

following parabolic Poiseuille profile $v(r) = Pe(1-r^2)$, where r is the radial coordinate and Pe is the Péclet number which quantify the ratio between convection/diffusion effects, and is taken equal to $Pe = 10$ is the following. All conductivities in the fluid and the solid are equal to unity. In the following, all the solid inlet/outlet conditions are homogeneous Neumann. Inlet/outlet conditions in the fluid sub-domains are the following

- **Test case 1:** prescribed temperature $T = 1$ at the inlet on $\Gamma_D^I = \Omega^1 \times \{0\}$ and Robin condition $\partial_z T + \alpha v(\xi) T = 0$ at the outlet $\Gamma_R^O = \Omega^1 \times \{L\}$, as depicted on Fig. 2, and with $\alpha = 1/(k_f Pe)$ ($k_f = 1$ denoting the fluid thermal conductivity). This condition expresses a balance between the convective and diffusive heat flux at the outlet, it models a free boundary output condition.
- **Test case 2:** prescribed temperature $T = 1$ at the inlet on Γ_D^I, coupling (4) with an outlet tube on $\Gamma_C^O = \Omega^1 \times \{L\}$, as depicted on Fig. 3. In this case the temperature $T^{+\infty}$ at $z = +\infty$ in the outlet tube is an unknown.
- **Test case 3:** Coupling with both inlet and outlet tubes using (4) at $\Omega^1 \times \{0\}$ and $\Omega^1 \times \{L\}$, as depicted on Fig. 4. In this case the temperature condition $T = 1$ in the inlet $\Omega^1 \times \{0\}$ is replaced by a prescribed temperature $T^{-\infty} = 1$ at $z = -\infty$ in the inlet tube, as previously $T^{+\infty}$ in the outlet tube is an unknown.

For each test case the linear system $\mathbf{M}_{\mathcal{L}_2} x = \mathbf{b}$ in (7) is assembled as presented in Sections 2.2, 2.3 and 2.4 respectively to test cases 1, 2 and 3. It is then solved, providing the minimizer T_N of the functional $J_{\mathcal{L}_2}$ over the space V_N. The spaces V_N will always be set so that $N^+ = N^- = N^O = N^I := \overline{N}$. The modal convergence of the method will be investigated with respect to this parameter $\overline{N}$. The total dimension of V_N respectively equals $N = 2\overline{N}$, $N = 3\overline{N}+1$ and $N = 4\overline{N}+1$ in test case respectively 1, 2 and 3.

The minimizer $T_{\overline{N}}$ will be computed for $\overline{N}$ varying between 1 and 35 for test case 1 and between 1 and 28 for test cases 2 and 3. This allows us to analyze the behavior of $J_{\mathcal{L}_2}(T_{\overline{N}})$ as $\overline{N}$ increases. Two other quantities of physical interest will be computed using $T_{\overline{N}}$: the fluid/solid heat flux denoted $\phi(\overline{N})$ in the heat exchanger, (i.e. the flux on the interface $\partial\Omega^1 \times (0, L)$) and the temperature as $z = +\infty$ in the outlet tube denoted $T_\infty(\overline{N})$, precisely

$$\phi(\overline{N}) = \int_0^L \int_{\partial\Omega^1} -k\nabla T_{\overline{N}} \cdot \mathbf{n}\, dl\, dz,$$
$$\& \; T_\infty(\overline{N}) = \lim_{z \to +\infty} T_{\overline{N}}.$$

The limits ϕ and T_∞ for these two sequences represent the fluid/solid flux in the heat exchanger and the temperature at $z = +\infty$ in the outlet tube for the exact solution T to the considered problem. These limits ϕ and T_∞ have been evaluated, and the relative errors due to truncation are computed as,

$$e_\phi(\overline{N}) = \frac{|\phi(\overline{N}) - \phi|}{|\phi|}, \qquad e_{T_\infty}(\overline{N}) = \frac{|T_\infty(\overline{N}) - T_\infty|}{|T_\infty|}.$$

Our aim is to analyze the asymptotic behavior of $J_{\mathcal{L}_2}(T_{\overline{N}})$, $e_\phi(\overline{N})$ and $e_{T_\infty}(\overline{N})$ as $\overline{N} \to +\infty$.

The convergence of $J_{\mathcal{L}_2}(T_{\overline{N}})$ is illustrated in Fig. 6 (right) for test case 1 and in Fig. 7 for the test cases 2 and 3. The observed similar linear behavior in bi-logarithmic scale suggest that $J_{\mathcal{L}_2}(T_{\overline{N}})$ converges as $O(N^{-3/2})$. Nevertheless, each component of the functional displays its own convergence rate and the resulting overall trend is dominated by the worse converging component which is the term associated with the prescribed Dirichlet or the coupling temperature continuity between the inlet/outlet and the heat exchanger.

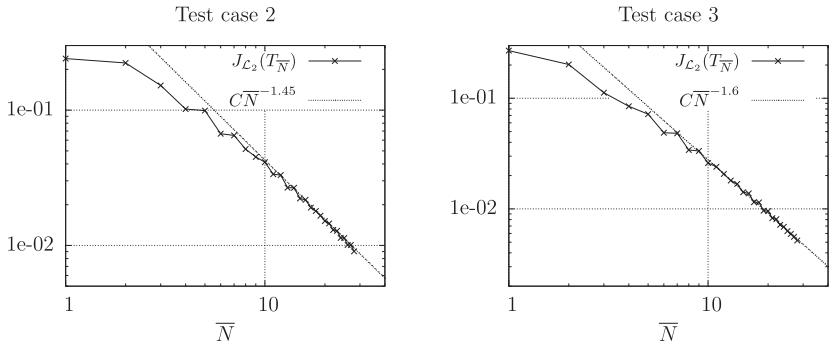

Fig. 7. Convergence of $J_{\mathcal{L}_2}(T_N)$ toward 0 versus N_{modes} in bi-logarithmic scale for test cases 2 and 3.

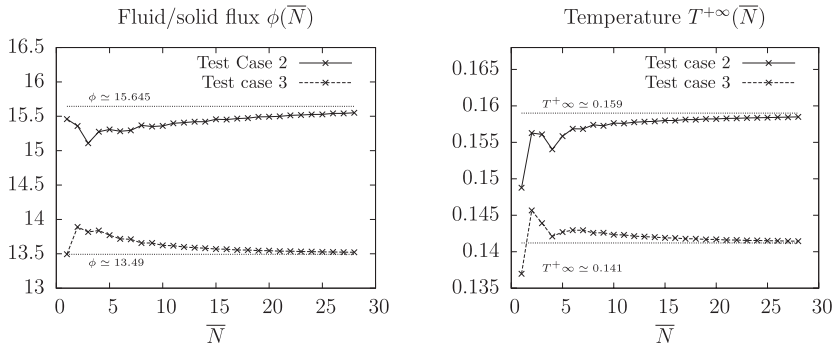

Fig. 8. Convergence of the predicted fluid/solid flux $\phi(\overline{N})$ (on the left) and of the predicted temperature $T_\infty(\overline{N})$ (on the right) for the test cases 2 and 3.

Table 1
Relative errors $e_\phi(\overline{N})$ and $e_{T_\infty}(\overline{N})$ associated with the computed fluid/solid flux and computed temperature at $z=+\infty$ respectively on the left and on the right.

$e_\phi(\overline{N})$			
N	Case 1	Case 2	Case 3
1	0.064	0.012	0 (*sic*)
2	0.049	0.018	0.03
3	0.046	0.034	0.024
5	0.034	0.022	0.02
8	0.025	0.018	0.012
11	0.021	0.016	0.009

$e_{T_\infty}(\overline{N})$		
N	Case 2	Case 3
1	0.064	0.030
2	0.017	0.030
3	0.018	0.019
5	0.020	0.010
8	0.010	0.010
11	0.009	0.008

The convergence of the fluid/solid flux ϕ is illustrated in Fig. 6 (right) for test case 1 and in Fig. 8 (left) for the test cases 2 and 3. All test cases exhibit a rather slow convergence rate with $\overline{N}$: test case 1 has the slowest convergence whereas test case 3 has the fastest. The examination of the relative error $e_\phi(\overline{N})$ shows a geometric convergence $e_\phi(\overline{N}) = O(\overline{N}^{-\alpha})$ with $\alpha \simeq 0.85$, $\alpha \simeq 1$ and $\alpha \simeq 1.5$ for test case 1, 2 and 3 respectively. Relative errors $e_\phi(\overline{N})$ are given in Table 1: even with a very small number of considered Graetz modes $\overline{N}$, the error is within a few percent and is less than 1 percent with 10 modes.

The convergence of the temperature T_∞ at $z=+\infty$ is illustrated in Fig. 8 (right) for the test cases 2 and 3. The asymptotic behavior of the relative error $e_{T_\infty}(\overline{N})$ has also a geometric behavior, $e_{T_\infty}(\overline{N}) = O(\overline{N}^{-\alpha})$ with $\alpha \simeq 1$ and $\alpha \simeq 1.5$ for test cases 2 and 3 respectively. Again, although this convergence rate appears as rather slow, it only holds in the asymptotic region: as displayed on Table 1, we obtained an accurate estimation of T_∞ (within a few percent) with very few Graetz modes, and below 1% with eight modes only.

3. Numerical illustrations

A first set of numerical examples has been developed in the previous Section 2.6 using an analytical (mesh-free) computation of the Graetz modes. This method however is restricted to axi-symmetric geometries. In this section we present numerical results obtained with a finite element formulation which holds for general geometries. Three cases are consid-

ered. Firstly we consider test cases 2 and 3 presented in Section 2.6 in order to validate the finite element solver. Secondly a non-axi-symmetric configurations, are also tested

- **Test case 4**: a cylindrical finite exchanger coupled with two upstream and two downstream tubes.
- **Test case 5**: a cylindrical finite exchanger coupled with four upstream and four downstream tubes.

The aim of these two additional test cases is to demonstrate that the proposed approach can address realistic complex 3D heat exchangers geometries, where the 3D temperature field and heat flux are reconstructed.

3.1. Discrete finite element formulation

The first computational step is the evaluation of the generalized Graetz modes $T_n^{\pm}$ and of the associated eigenvalues relatively to each transverse domains Ω^k, $k \geqslant 0$. We recall the generalized (quadratic) eigenvalue problem in Definition 1.2 satisfied by the Graetz modes:

$$\begin{aligned} &\operatorname{div}(k\nabla T_\lambda) + k\lambda^2 T_\lambda = v\lambda T_\lambda \quad \text{on } \Omega, \\ &T_\lambda(\xi)_{|\partial\Omega=0} \quad \text{or} \quad k\nabla T_\lambda(\xi)_{|\partial\Omega=0} \cdot \mathbf{n} = 0 \end{aligned}$$

Where Ω either denotes the heat exchanger section Ω^0 (in which case the boundary condition on $\partial\Omega$ is the homogeneous Dirichlet one) or an input/output semi-infinite tube section Ω^k ($k \geqslant 1$, in which case the boundary condition on $\partial\Omega$ is the homogeneous Neumann one). We simply focus here on the generic computation of the λ, T_λ. We present the method in the Dirichlet case as in [22].

As developed in [21], this quadratic eigenvalue problem can be reformulated into a linear (classical) eigenvalue problem by introducing the supplementary unknown $\mathbf{F}$, which is a vector function on Ω. Precisely, we search for $\begin{vmatrix} T \\ \mathbf{F} \end{vmatrix}$ and for $\lambda \in \mathbb{R}$ so that,

$$\begin{vmatrix} k^{-1}vT - k^{-1}\operatorname{div}(\mathbf{F}) \\ k\nabla T \end{vmatrix} = \lambda \begin{vmatrix} T \\ \mathbf{F} \end{vmatrix}.$$

It has been shown in [22] that the vector function $\mathbf{F}$ could be searched under the form $\mathbf{F} = k\nabla U$ for some scalar function $U \in H^1(\Omega)$. As a result we search for $(T, U) \in H_0^1(\Omega) \times H^1(\Omega)$ and for $\lambda \in \mathbb{R}$ so that for all test functions $(t, u) \in H_0^1(\Omega) \times H_0^1(\Omega)$ we have,

$$a_1\big[(T, U), (t, u)\big] = \lambda a_2\big[(T, U), (t, u)\big],$$

where the bilinear products a_1 and a_2 are defined by,

$$\begin{aligned} a_1\big[(T, U), (t, u)\big] &= \int_\Omega (vTt + k\nabla T \cdot \nabla u + k\nabla t \cdot \nabla U)\, dx, \\ a_2\big[(T, U), (t, u)\big] &= \int_\Omega (kTt + k\nabla U \cdot \nabla u)\, dx. \end{aligned}$$

This problem is approximated using the space $P^k(\mathcal{M})$ of Lagrange-P^k finite elements (for $k = 1$ or 2) on a triangulation $\mathcal{M}$ of Ω, as exemplified in Fig. 9. The discrete formulation reads as follows: find $(T_h, U_h) \in P_0^k(\mathcal{M}) \times P_0^k(\mathcal{M})$ and $\lambda \in \mathbb{R}$ so that for all test functions $(t, u) \in P_0^k(\mathcal{M}) \times P_0^k(\mathcal{M})$ we have,

$$a_1\big[(T_h, U_h), (t, u)\big] = \lambda a_2\big[(T_h, U_h), (t, u)\big],$$

and where $P_0^k(\mathcal{M})$ denotes the sub-space of $P^k(\mathcal{M})$ composed of all functions vanishing on $\partial\Omega$. The discrete problems takes the form of the following linear system,

$$\mathbf{A}_1 \begin{vmatrix} T_h \\ U_h \end{vmatrix} = \lambda \mathbf{A}_2 \begin{vmatrix} T_h \\ U_h \end{vmatrix}, \tag{21}$$

where $\mathbf{A}_1$ and $\mathbf{A}_2$ respectively are the matrix for the bilinear products a_1 and a_2 restricted to $P_0^k(\mathcal{M}) \times P_0^k(\mathcal{M})$ and written considering their classical bases. In practice, assembling $\mathbf{A}_1$ and $\mathbf{A}_2$ only requires to assemble classical mass and stiffness matrix following the definition of a_1 and a_2. This is done using the finite element library *FreeFem++* [30]. The resolution of the general eigenvalue problem (21) is performed using library *arpack++* [31].

The adaptation of this method to the Neumann case has been further developed in [23]. The numerical implementation is quite similar here but for test functions space which differs from [23]. One has to solve (21) with $\mathbf{A}_1$ and $\mathbf{A}_2$ alternatively defined as the matrix for the bilinear products a_1 and a_2 restricted to $P^k(\mathcal{M}) \times P^k(\mathcal{M})$.

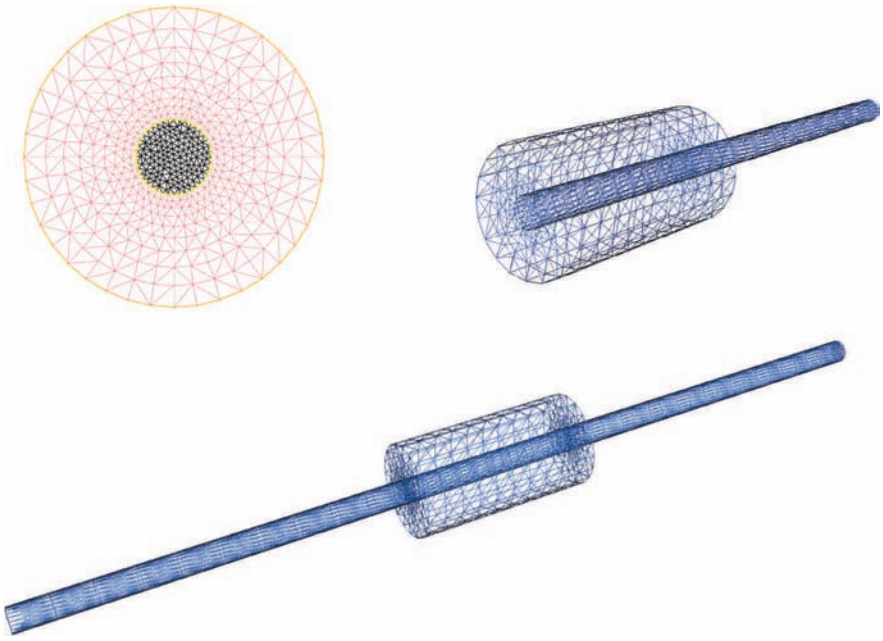

Fig. 9. Upper left: illustration of the triangle meshes generated by FreeFem++ for test cases 2 and 3. The mesh in black is the triangulation of Ω^1 (fluid sub-domain) and the one in red is the triangulation of $\Omega^0 - \Omega^1$ (solid sub-domain). The represented meshes are intentionally poorly refined in order to illustrate the conformal connection of the two meshes at the circular frontier $\partial\Omega^I$ (in yellow). Upper right and lower sub-figures: 3D meshes obtained from the extrusion of the upper left 2D mesh generated in order to visualize the complete reconstructed solution in the x, y, z directions for test cases 2 (upper right) and 3 (lower figure). (For interpretation of the references to color in this figure legend, the reader is referred to the web version of this article.)

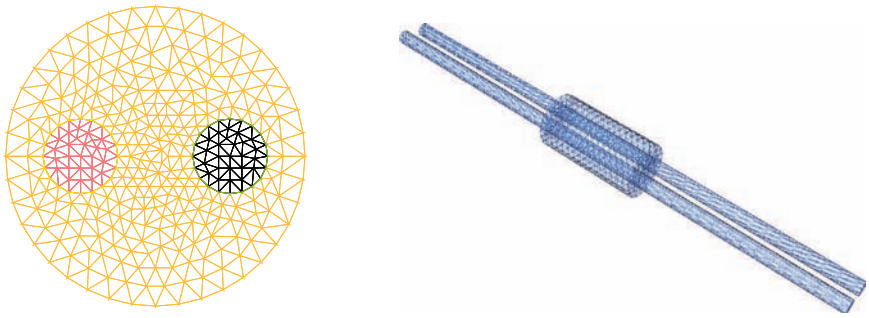

Fig. 10. Left sub-figure: Illustration of the finite element mesh generated by FreeFem++ in domain Ω^0 for test case **4**. Right sub-figures: 3D mesh obtained from the extrusion of the upper 2D mesh for 3D reconstruction and visualization of the solution.

The second computational step consists in building the matrix $\mathbf{M}_{\mathcal{L}_2}$ and the right-hand-side $\mathbf{b}$ in (7) associated with the discrete minimization problem 2.1. Depending on the configuration at ends, this building necessitates various sub-matrix to be evaluated as discussed in Section 2.1 i.e. $\mathbf{K}$ in (10) and $\mathbf{Q}$, $\mathbf{R}$, and $\mathbf{S}$ in (16). In general, the coefficients of those sub-matrix involve evaluation of integrals of type

$$\int_{\Omega^0} T_i(\xi) T_j(\xi)\, dx, \qquad \int_{\Omega^k} t_i(\xi) t_j(\xi)\, dx \quad \text{or} \quad \int_{\Omega^k} T_i(\xi) t_j(\xi)\, dx,$$

where the $T_{i,j}$ denote Graetz modes associated with the heat exchanger on Ω^0 and where the $t_{i,j}$ denotes Graetz modes associated with one given semi-infinite tube on Ω^k, $k = 1, 2$. As illustrated on Figs. 9 and 10, the mesh for Ω^k is a conformal sub-mesh of the mesh $\mathcal{M}$ for Ω^0. As a result it is possible (and quite simple) to consider all functions $T_{i,j}$ and $t_{i,j}$ as elements of $P^k(\mathcal{M})$, by extending $t_{i,j}$ to 0 outside Ω^k, i.e. it is set equals to zero in the solid interface in $\Omega^0 \setminus \bigcup_{k>0} \Omega^k$. All these integral products can then be computed easily from considering the mass matrix $\mathbf{M}_\Omega$ on $P^k(\mathcal{M})$ and by performing the products,

$$T_i^T \mathbf{M}_\Omega T_j, \quad t_i^T \mathbf{M}_\Omega t_j \quad \text{or} \quad T_i^T \mathbf{M}_\Omega t_j. \tag{22}$$

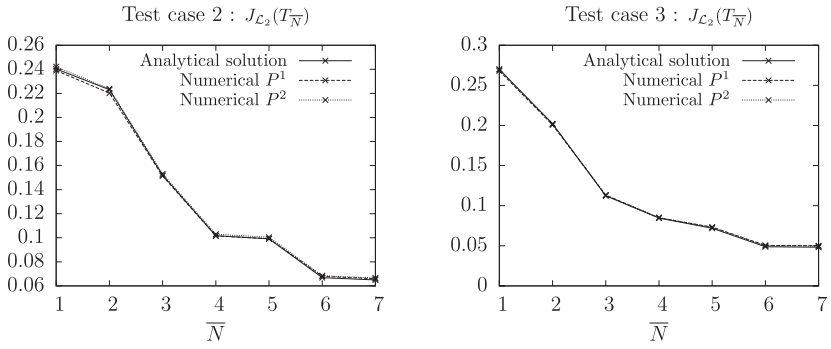

Fig. 11. Mode convergence for functional $J_{\mathcal{L}_2}(\overline{N})$ using finite element discretization $P1$ & $P2$ versus the mode truncation order $\overline{N}$ for case **2** (left) and case **3** (right) configurations.

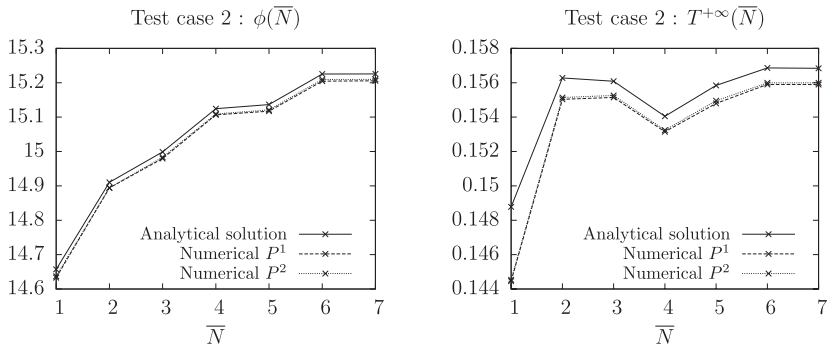

Fig. 12. Mode convergence for the flux fluid/solid $\phi(\overline{N})$ (left) and the temperature $T_{+\infty}(\overline{N})$ (right) using finite element discretization $P1$ & $P2$ versus the mode truncation order $\overline{N}$ for case **2** configuration.

The numerical cost for assembling the four matrix **K** (10), **Q**, **R**, and **S** in (16) is therefore one sparse matrix/vector product each. This is thus quite light: the assembling of the mass matrix $\mathbf{M}_\Omega$ is furthermore required for evaluating $\mathbf{A}_2$ in (21) and does not need to be repeated here.

The overall computational algorithm thus reads as follows:

1. Define the heat exchanger domain Ω^0 and the inlet/outlet sub-domains Ω^k, then mesh each domain in a conformal way (i.e. so that the meshes of the Ω^k are sub-meshes of Ω^0's mesh).
2. Define the inlet/outlet conditions (prescribed boundary conditions (3) and/or inlet/outlet coupling (4) with semi-infinite tubes) and form the space V of solutions as described in Sections 2.2 to 2.5.
3. Construct the Graetz modes and the associated eigenvalues for each domain Ω^k ($k \geqslant 0$) using (21) consistently with the space V definition.
4. Built **K** from (10), **Q**, **R**, and **S** from (16) using the mass matrix $\mathbf{M}_\Omega$ as detailed in (22).
5. Built $\mathbf{M}_{\mathcal{L}_2}$ and the right-hand-side **b** in (7) and invert $\mathbf{M}_{\mathcal{L}_2}\mathbf{x} = \mathbf{b}$.
6. Reconstruct the complete solution from the chosen solution space V from the resulting eigenmode decomposition **x**.

3.2. Finite element solver evaluation

In this sub-section we consider the axi-symmetric test cases 2 and 3 presented in Section 2.6 within the same setting. We perform the same simulations as in Section 2.6 using both P^1 and P^2 finite elements. The purpose of this section is to validate the finite element method on this axi-symmetric configuration from comparison with the analytical results of Section 2.6.

The minimizers $T_{\overline{N}}$ have been computed for $1 \leqslant \overline{N} \leqslant 7$. We hereby present the convergence results of functional minimization $J_{\mathcal{L}_2}(T_{\overline{N}})$, infinite temperature $T_\infty(\overline{N})$ and exchange flux at the fluid/solid interface $\phi(\overline{N})$.

We observe from Fig. 11, Figs. 12 and 13 inspection that the two finite element discretization show very few difference with the analytical predictions. The functional convergence to zero is thus also observed with finite element discretization.

The predicted temperature at infinity $T_\infty(\overline{N})$ observed in Figs. 12 and 13 tends to an asymptotic limit as $\overline{N}$ increases. The comparison between analytical predictions and numerical estimates are close within 1% for P^1 and smaller than 1% for P^2.

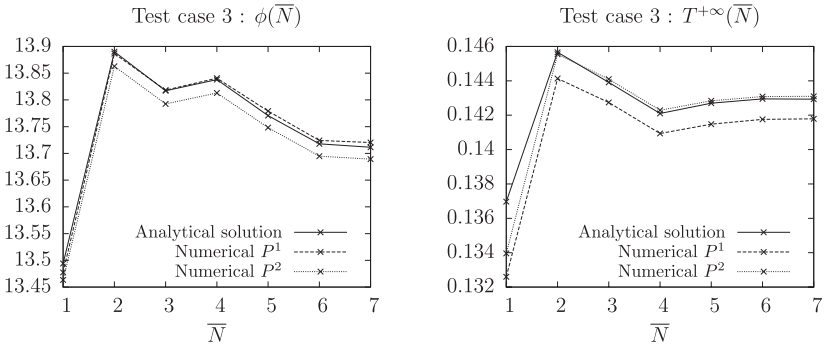

Fig. 13. Mode convergence for the flux fluid/solid $\phi(\overline{N})$ (left) and the temperature $T_{+\infty}(\overline{N})$ (right) using finite element discretization $P1$ & $P2$ versus the mode truncation order $\overline{N}$ for case **3** configuration.

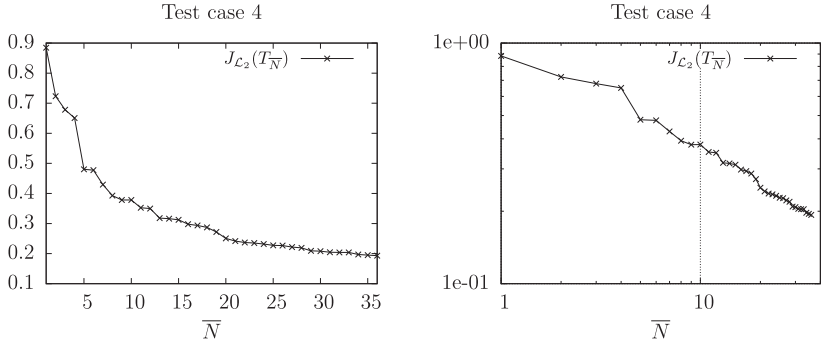

Fig. 14. Mode convergence for functional $J_{\mathcal{L}_2}(\overline{N})$ toward zero (left) and using log–log coordinates (right) versus the mode truncation order $\overline{N}$ for case **4** configuration.

The same conclusion holds for the predicted fluid/solid flux $\phi(\overline{N})$. The finite element solver is thus fully validated by this comparison.

3.3. Illustration on realistic heat exchangers geometry

3.3.1. Two inlets and two outlet

In this section we consider the case of a finite heat exchanger coupled with two Inlet/Outlet semi-infinite counter-current tubes. This configuration is precisely described on Fig. 5 and the mesh geometry is depicted on Fig. 10. The heat exchanger domain Ω^0 is a circle of radius equals to 4 whose center C is chosen as the origin of coordinates. The Inlet/Outlet domains $\Omega^{1,2}$ are unit radius circles whose center are symmetrically placed at position $(\pm 3/2, 0)$ from center C in domain Ω^0. We chose the heat exchanger length $L = 12$ and the Péclet number Pe is chosen equals to $Pe = 5$ and $Pe = 50$. The two input temperatures associated with the cold and hot Inlets T_{ic}, and T_{ih} are imposed. Two free output temperature have to be found at the far hot and cold tube outlets T_{oc}, and T_{oh}. We denote the imposed wall temperature T_w on the heat exchanger boundary $\partial\Omega^0 \times (0, L)$. We hereby use the dimensionless temperature $\tilde{T}_a = (T - T_w)/(T_{ic} - T_w)$, so that the wall temperature is reset to zero in this dimensionless formulation and the dimensionless input-hot temperature is set to $\tilde{T}_{ih} = 1$. Thus, there is only one input parameter, the dimensionless cold inlet temperature $\tilde{T}_{ic} = (T_{ic} - T_w)/(T_{ih} - T_w)$.

Fig. 14 shows that, in this case, the functional also decreases to zero when increasing the mode truncation, as expected. Furthermore we also illustrate a two-dimensional reconstruction of the temperature field in a transverse/longitudinal plane defined by the three axial center of the two inlet and outlet tubes and the heat exchanger. The temperature is thus reconstructed in the three-dimensional mesh illustrated in Fig. 9 and then represented within a plane for illustration in Fig. 15. Two distinct Péclet number equal to $Pe = 5$ and $Pe = 50$ have been chosen in Fig. 15 to illustrate the applicability of the method for low and a strong convective regime. The input-cold temperature is set to $\tilde{T}_{ic} = -1$, which corresponds to a symmetrical configuration where the inlet hot and cold temperature are symmetrically distant from the wall temperature. Fig. 15 has been scale so that the exchanger length is different in the upper and middle sub-figure, but exactly adapted to the first eigenvalue. The very small difference observed between the upper and middle sub-figure temperature profile illustrates that when convection is dominant, the temperature reaches a fully developed solution which can be encapsulated in a properly rescaled longitudinal variation given by the first eigenvalue λ_1 which indeed depends on Pe. This fully developed regime is the same as the one obtained in the classical Graetz solution in a tube, except that, here, both upstream and downstream directions are concerned. The exchanger capacity will be examined along these lines in the next paragraph.

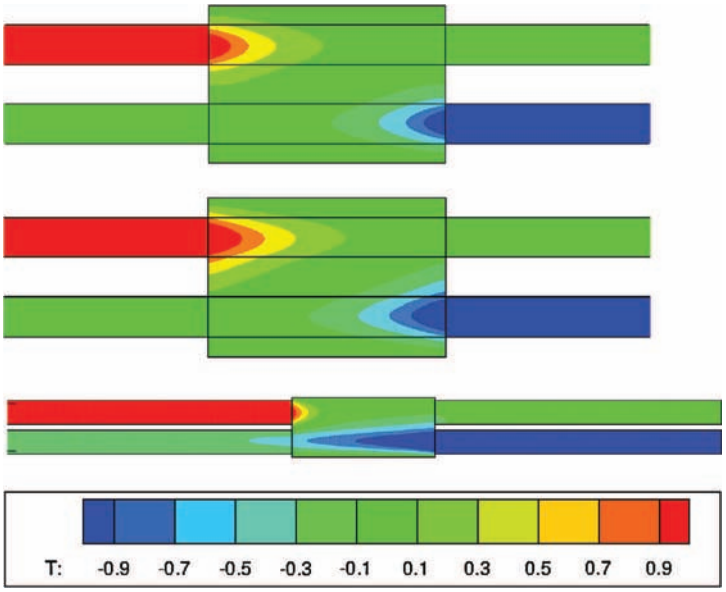

Fig. 15. Comparison of the temperature field within the heat exchanger for three configurations with dimensionless cold input temperature $\tilde{T}_{i,c} = -1$. The upper figure, is a symmetrical configuration where both $Pe = 5$ and an exchanger length equals $L = 3\lambda_1$ where λ_1 is the first eigenvalue. The middle figure, also corresponds to a symmetrical configuration with $Pe = 50$ and an exchanger length $L = 3\lambda_1$. For both upper and middle sub-figures the external diameter of the exchanger is 5. The lower figure corresponds to a non-symmetrical flux configuration with $Pe = 5$ on the upper tube, $Pe = 50$ on the lower one for exchanger length $L = 12$. For this lowest sub-figure, the external diameter of the exchanger is 2.5. For all sub-figures the distance between internal tubes centers is 2.5, whilst heir inner radius diameter equals 1.

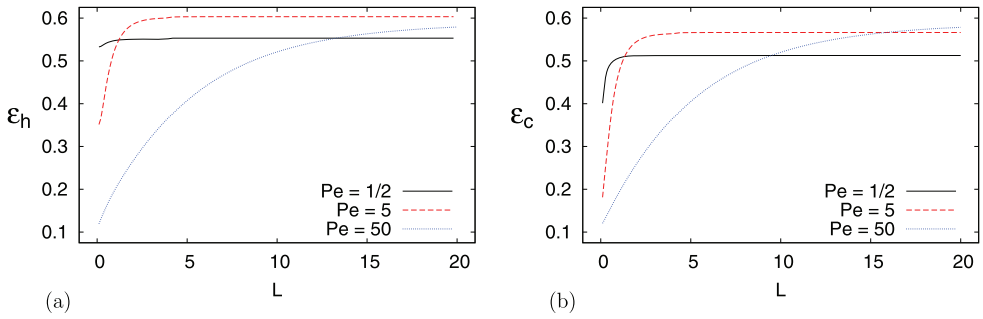

Fig. 16. Considering a heat exchanger with external circular Ω^0 radius equals to 4, and Inlet/Outlet domains $\Omega^{1,2}$ of unit circles radius whose center are symmetrically placed at position $(\pm 3/2, 0)$ with dimensionless input cold source equals to $\tilde{T}_{ic} = -1$, we compute the heat exchange effectiveness variation versus the exchanger length L for three different value of the Péclet number in (a) for ϵ_h in (b) for ϵ_c.

Finally Fig. 15 also illustrates in the lower sub-figure, the example of a non-symmetrical hydrodynamic situation where the convective effects is ten times smaller in the upper tube than in the lower one, resulting in more elongated temperature gradient, downstream.

We now illustrate the usefulness of the method by computing the heat exchange effectiveness (consistent with notations used in [1])

$$\epsilon_h = \frac{T_{i,h} - T_{o,h}}{T_{i,h} - T_{i,c}} \quad \& \quad \epsilon_c = \frac{T_{o,c} - T_{i,c}}{T_{i,h} - T_{i,c}},$$

where index h in ϵ_h refers to the heat exchanger ability for cooling the hot fluid, and similarly index c in ϵ_c stands for the heat exchange effectiveness for heating-up the cold fluid. It is interesting to observe in Fig. 16 that the heat exchange effectiveness saturates for a given length, which means that the ability to heat-up the input fluid or conversely cool-down the output one, hardly exceed, in the considered configuration, 60% of the maximum temperature difference between the hot and cold sources. Not only the heat exchange effectiveness saturates with the exchanger length but also with the Péclet number. Increasing convective effects from raising the Péclet number enlarges the exchanger length for which the exchange effectiveness reaches saturation, as can be observed in Fig. 16. Nevertheless, it merely affects the maximum accessible efficiency. It is also interesting to observe that even for Péclet number as small as 1/2, the maximum accessible exchange efficiency can reach 50%. Hence, for sufficiently well designed exchanger length, increasing the convection by two order

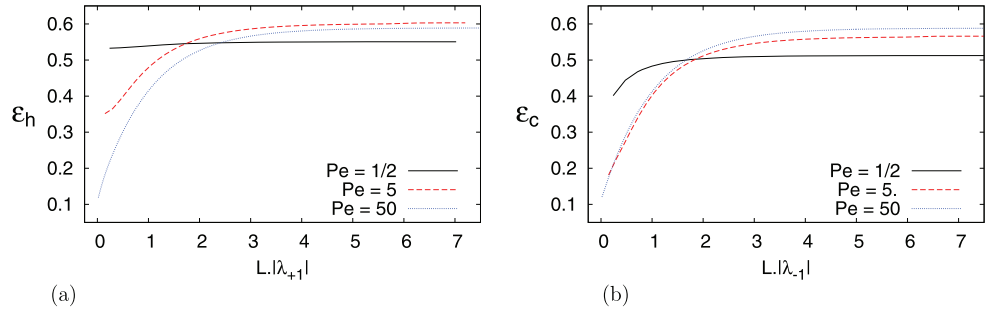

Fig. 17. Same convention as in Fig. 16 except that the results are plotted versus re-normalized length $L.\lambda_{\pm 1}$ where the first eigenvalue $\lambda_{\pm 1}$ provide the inverse of the typical longitudinal upstream or downstream temperature variations.

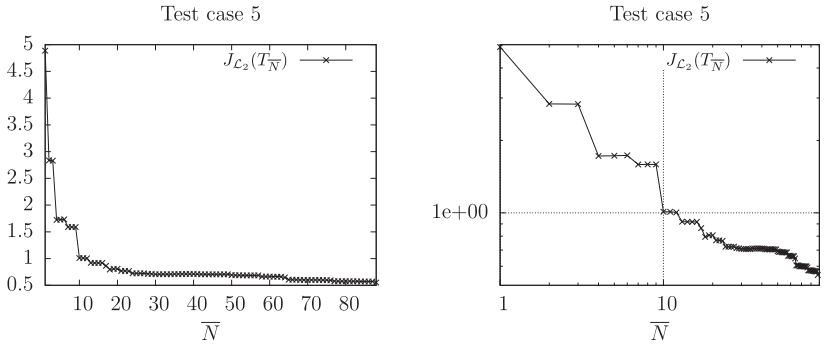

Fig. 18. Mode convergence for functional $J_{\mathcal{L}_2}(\overline{N})$ toward zero (left) and using log–log coordinated (right) versus the mode truncation order $\overline{N}$ for case **5** configuration.

of magnitude will not permit to get more than 5% in exchange efficiency. This illustrate that varying the geometrical and physical parameters provides very useful prediction for the exchanger functional capacities. Finally it is then interesting to re-plot Fig. 16 data versus a re-normalized exchanger length since, it provides a very nice collapse of the exchanger effectiveness curves obtained for large Péclet in Fig. 17. This result can be understood in direct analogy with classical Graetz analysis for which a fully developed thermal regime is reached at high Péclet number. In this case, the cooling and heating exchange effectiveness are respectively dominated by the downstream or upstream longitudinal variations given by the first downstream or upstream eigenvalue associated with the exchanger generalized Graetz problem. This observation also showcases that the relevant parameters are embedded in the chosen generalized Graetz formulation. As a final remark, we can also observe that, in the case illustrated here of an exchanger with prescribed wall temperature, the final effectiveness of the exchanger is mainly controlled by the thermal conditions (it is most effective when inlet and outlet temperature are symmetrical with the imposed one at the wall) but weakly depends on the imposed hydrodynamics since a fully developed regime merely increases the effectiveness by 10%.

3.3.2. Four inlets and four outlets

We illustrate in this section a more complex example of realistic exchanger with four inlet/outlet circular tubes. In this case, using the general formulation 2.5 we compute the resulting functional which also decreases to zero, with an algebraic convergence rate as illustrated in Fig. 18. In this more complex case, the computation provides all the previously computed quantities such as, exchange fluxes, output temperature, exchanger efficiency, etc. In this section our goal is rather to illustrate some physical insights about the computed solution and provide the evidence that our formulation has very good abilities to study configurations having many inlets. For this purpose, we evaluate the temperature iso-values at three different transverse plane in the entrance, the middle and the exit of the exchanger.

When choosing a convection dominant situation with $Pe = 5$, with an alternative counter-current input temperature $\tilde{T}_{i,c} = \pm 1$, one can observe in Fig. 19 that the temperature gradients are localized at the frontier between counter-current tube couples. This is especially true nearby the entrance ($z = L/4$) or the exit ($z = 3L/4$). On the contrary, in the middle of the exchanger ($z = L/2$), one can observe that the gradients are much less marked, and the imposed temperature at the exchanger frontier is almost imprinted inside the closest tubes to the wall which have been “thermalized” by the exchanger.

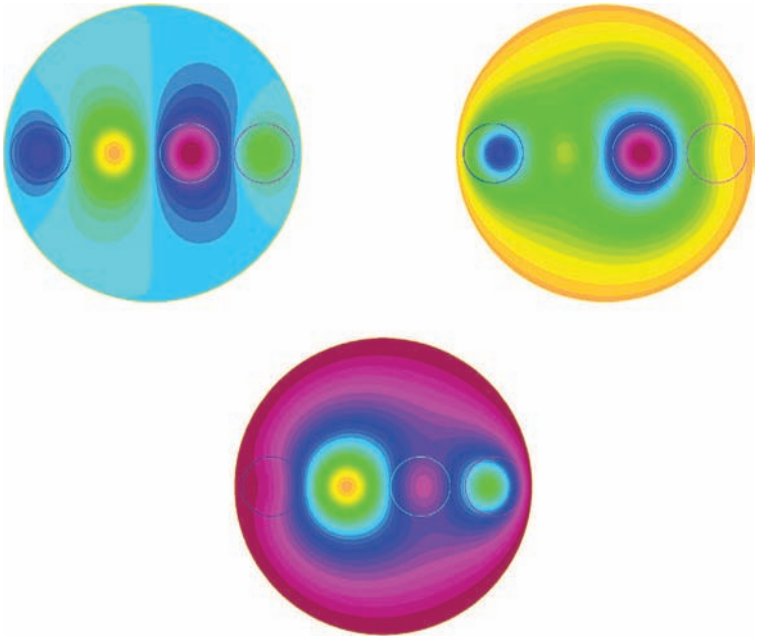

Fig. 19. Temperature iso-values inside an exchanger having four inlet/outlet in three different (x, y) planes. The upper left sub-figure corresponds to a cut into $z = L/4$ plane, the upper right one to $z = L/2$ and the lower one to $z = 3L/4$. The four tube inlets have unit diameters, the frontier of which are represented by four circles. The exchanger radius equals 5 and the distance between tubes is 2.5. A counter-current injection with $Pe = 5$ is chosen, so that from left to right the injection is imposed from $z \to -\infty$ to $z \to +\infty$ in the first tube, from $z \to +\infty$ to $z \to -\infty$ in the second one, from $z \to -\infty$ to $z \to +\infty$ in the third one, and $z \to +\infty$ to $z \to -\infty$ in the far right one.

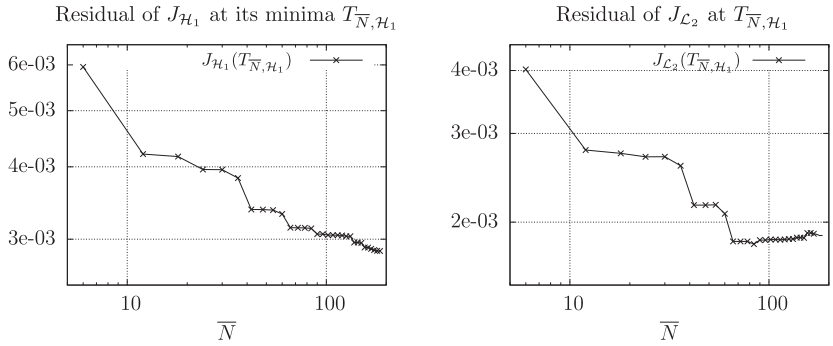

Fig. 20. Test of the mode convergence between the $\mathcal{H}_1$ and the $\mathcal{L}_2$ functional for test case **4**. The left figure provides the residual associated with functional $J_{\mathcal{H}_1}$ defined in (23) versus the mode number N, which could be compared with the convergence observed in Fig. 14 for $J_{\mathcal{L}_2}$. The right figure provides the residual of the $J_{\mathcal{L}_2}$ functional associated with the solution obtained using $J_{\mathcal{H}_1}$.

3.4. Test of H_1 functional versus $\mathcal{L}_2$

This section discusses the ability to consider a different functional $J_{\mathcal{H}_1}$ based upon the $\mathcal{H}_1$ norm between the inlet and the outlet compartments. This new functional differs from the previous one $J_{\mathcal{L}_2}$ defined in (6) by

$$J_{\mathcal{H}_1}(T) = J_{\mathcal{L}_2}(T) + \int_{\Gamma_C} \nabla(T_{\text{left}} - T_{\text{right}}) \cdot \nabla(T_{\text{left}} - T_{\text{right}})\, ds \tag{23}$$

As in paragraph 2.1, this new functional is associated with a new linear system

$$\mathbf{M}_{\mathcal{H}_1}\mathbf{x} = \mathbf{b}. \tag{24}$$

In Fig. 20, we denote $\mathbf{x}_{\mathcal{H}_1}$ the solution obtained from the inversion of (24) and $\mathbf{x}_{\mathcal{L}_2}$ from the inversion of (7).

Building matrix $\mathbf{M}_{\mathcal{H}_1}$ closely follows the steps described in Sections 2.2, 2.4 and 3.1. Changes in building the matrix system is concentrated into changes in (16) involving additional terms of the type $\int \nabla T_i \cdot \nabla T_j\, ds$. More specifically, matrix $\mathbf{Q}_{ab}$ $\mathbf{R}_{a+}$ and $\mathbf{S}_{+}$ should be changed into $\mathbf{Q}_{ab}^{\mathcal{H}_1}$ $\mathbf{R}_{a+}^{\mathcal{H}_1}$ and $\mathbf{S}_{+}^{\mathcal{H}_1}$ as follows:

$$\mathbf{Q}_{ab}^{\mathcal{H}_1}(i,j) = \mathbf{Q}_{ab}(i,j) + \int_{\Gamma_c} \nabla T_i^a \cdot \nabla T_j^b \, ds$$

$$\text{for} \quad 1 \leqslant i \leqslant N^a, \; 1 \leqslant j \leqslant N^b,$$

$$\mathbf{R}_{a+}^{\mathcal{H}_1}(i,j) = \mathbf{R}_{a+}(i,j) + \int_{\Gamma_c} \nabla T_i^a \cdot \nabla t_j^+ \, ds,$$

$$\text{for } 1 \leqslant i \leqslant N^a \text{ and } 0 \leqslant j \leqslant N^{\nabla} t_j^+ \, ds,$$

$$\text{for } 1 \leqslant i \leqslant N^a \text{ and } 0 \leqslant j \leqslant N^O,$$

$$\mathbf{S}_{+}^{\mathcal{H}_1}(i,j) = \mathbf{S}_{+}(i,j) + \int_{\Gamma_c} \nabla t_i^+ \cdot \nabla t_j^+ \, ds, \quad \text{for } 0 \leqslant i,j \leqslant N^O. \tag{25}$$

The implementation and the finite element assembling procedure exposed in Section 3.1 should be repeated here, with this new functional, except that one should now build matrix $M_{\mathcal{H}_1}$. Using this new formulation, we compare the computations of test case **4**, associated with two inlet/outlet tubes. One can observe in Fig. 20-left that the convergence of this $\mathcal{H}_1$ functional is slower than the one observed in Fig. 14 for the $\mathcal{L}_2$ one. This result is expected since this functional $J_{\mathcal{H}_1}$ involves supplementary positives terms that cannot produce an increased convergence. More interestingly, Fig. 20-right shows that evaluating the functional $J_{\mathcal{L}_2}$ on the solutions $\mathbf{x}_{\mathcal{H}_1}$ obtained using the functional $J_{\mathcal{H}_1}$ also produces a residual converging to zero (it reaches 10^{-3} for 190 modes). This result gives support to the choice of the functional $J_{\mathcal{L}_2}$ providing a consistent result with the $J_{\mathcal{H}_1}$ functional, which is more mathematically relevant in our context.

4. Conclusions

We propose a new approach for the computation of parallel convective heat exchangers having complex configurations. To our knowledge, the method proposed here consider for the first time, the free boundary nature of heat exchangers, and how to compute the coupling between inlet and outlet conditions. The use of generalized Graetz modes not only permits to map a 3D complex problem into a 2D generalized eigenvalue formulation. It also provides an explicit solution for the basis coefficients amplitude from the inversion of a simple linear system issued from a quadratic variational problem involving the continuity of the fields at the interface of different compartments of the exchanger. We provide the mathematical formulation and the numerical illustration of the proposed method for configurations of increasing complexity with prescribed wall temperature as done in [16,6]. Some final illustrations have been put forward to show-case the applicability for realistic complex heat exchangers, with prescribed lateral temperature on the side walls of the exchanger.

The proposed methodology also applies to convective mass exchangers, for which it is equally relevant [32]. As a final remark, most of the proposed methodology could very closely apply to adiabatic or Robin type lateral conditions, except for taking into account a supplementary longitudinally linearly varying mode [23]. This extension, which might provide more physically relevant lateral conditions is nevertheless beyond the scope of the present paper but should deserve close attention in future efforts.

References

[1] R.K. Shah, D.P. Sekulić, Fundamentals of Heat Exchanger Design, John Wiley and Sons, New Jersey, 2003.
[2] J. Kragh, J. Rose, T.R. Nielsen, S. Svendsen, New counter flow heat exchanger designed for ventilation systems in cold climates, Energy Build. 39 (2007) 1151–1158.
[3] R.J. Nunge, W.N. Gill, An analytical study of laminar counter flow double-pipe heat exchangers, AIChE J. 12 (1966) 279–289.
[4] R.J. Nunge, W.N. Gill, Analysis of heat or mass transfer in some countercurrent flows, Int. J. Heat Mass Transf. 8 (1965) 873–886.
[5] C. Ho, H. Yeh, W. Yang, Double-pass flow heat transfer in a circular conduit by inserting a concentric tube for improved performance, Chem. Eng. Commun. 192 (2005) 237–255.
[6] C.-D. Ho, H.-M. Yeh, W.-Y. Yang, Improvement in performance on laminar counterflow concentric circular heat exchangers with external refluxes, Int. J. Heat Mass Transf. 45 (2002) 3559–3569.
[7] H.M. Yeh, Numerical analysis of mass transfer in double-pass parallel-plate dialyzers with external recycle, Chem. Eng. Commun. 33 (2009) 815–821.
[8] T.J. Wei, H. Chii-Dong, C. Ching-Jung, Effect of ultrafiltration on the mass-transfer efficiency improvement in a parallel-plate countercurrent dialysis system, Desalination 242 (2009) 70–83.
[9] H.M. Yeh, Mass transfer in cross-flow parallel-plate dialyzer with internal recycle for improved performance, Chem. Eng. Commun. 198 (2011) 1366–1379.
[10] M. Vera, A. Liñán, Laminar counter flow parallel-plate heat exchangers: Exact and approximate solutions, Int. J. Heat Mass Transf. 53 (2010) 4885–4898.
[11] A. Dorfman, Z. Renner, Conjugate problems in convective heat transfer: review, Math. Probl. Eng. 2009 (2009), ID 927350.
[12] W. Qu, I. Mudawar, Experimental and numerical study of pressure drop and heat transfer in a single-phase micro-channel heat sink, Int. J. Heat Mass Transf. 45 (2002) 2549–2565.
[13] W. Qu, I. Mudawar, Analysis of three-dimensional heat transfer in microchannel heat sinks, Int. J. Heat Mass Transf. 45 (2005) 3973–3985.
[14] A. Weisberg, H.H. Bau, J.N. Zemel, Analysis of microchannels for integrated cooling, Int. J. Heat Mass Transf. 35 (1992) 2465–2474.
[15] A.G. Fedorov, R. Viskanta, Three-dimensional conjugate heat transfer in the microchannel heat sink for electronic packaging, Int. J. Heat Mass Transf. 43 (2000) 399–415.
[16] Hong Chungpyo, Asako Yutaka, Suzuki Koichi, Convection heat transfer in concentric micro annular tubes with constant wall temperature, Int. J. Heat Mass Transf. 54 (2011) 5242–5252.

[17] X. Chen, P. Han, A note on the solution of conjugate heat transfer problems using simple-like algorithms, Int. J. Heat Fluid Flow 21 (2000) 463–467.
[18] L. Skerget, M. Hribersek, G. Kuhn, Computational fluid dynamics by boundary domain integral method, Int. J. Numer. Methods Eng. 46 (1999) 1291–1311.
[19] J. Blobner, M. Hribersek, G. Kuhn, Dual reciprocity BEM-BDIM technique for conjugate heat transfer computations, Comput. Methods Appl. Math. 190 (2000) 1105–1116.
[20] R.A. Bialecki, P. Jurgas, G. Kuhn, Dual reciprocity bem without matrix inversion for transient heat conduction, Eng. Anal. Bound. Elem. 26 (2002) 227–236.
[21] C. Pierre, F. Plouraboué, Numerical analysis of a new mixed-formulation for eigenvalue convection–diffusion problems, SIAM J. Appl. Math. 70 (2009) 658–676.
[22] J. Fehrenbach, F. De Gournay, C. Pierre, F. Plouraboué, The generalized Graetz problem in finite domains, SIAM J. Appl. Math. 72 (2012) 99–123.
[23] J. Bouyssier, C. Pierre, F. Plouraboué, Mathematical analysis of parallel convective exchangers, Math. Models and Methods Appl. Sci. 24 (2014) 627–667.
[24] J. Fehrenbach, F. de Gournay, F. Plouraboué, Shape optimization for the generalized Graetz problem, Struct. Multidiscip. Optim., http://dx.doi.org/10.1007/s00158-013-1032-4.
[25] R. Dautray, J. Lions, Mathematical Analysis and Numerical Methods for Science and Technology, Springer-Verlag, Berlin, 1988.
[26] P. Ciarlet, J. Lions, Handbook of Numerical Analysis, North-Holland, Amsterdam, 1990.
[27] J.B. Aparecido, R.M. Cotta, Laminar flow inside hexagonal ducts, Comput. Mech. 6 (1990) 93–100.
[28] C. Canuto, A. Quarteroni, Spectral Methods, Encyclopedia of Computational Mechanics, Wiley Online Library, 1996.
[29] C. Pierre, F. Plouraboué, Generalised Graetz problem: analytical solutions for concentric or parallel configurations, preprint hal:00737549, http://hal.archives-ouvertes.fr/hal-00737549.
[30] O. Pironneau, F. Hecht, A. Le Hyaric, J. Morice, Freefem++, http://www.freefem.org/ff++/, 2013.
[31] F. Magalhaes Gomes, D. Sorensen, Arpack++, http://www.caam.rice.edu/software/ARPACK/, 1996.
[32] C. Gostoli, A. Gatta, Mass transfer in a hollow fiber dialyzer, J. Membr. Sci. 6 (1980) 133–148.